

Tuning the Conductivity of Nanocomposites through Nanoparticle Migration and Interface Crossing in Immiscible Polymer Blends: A Review on Fundamental Understanding

Reza Salehiyan¹, Suprakas Sinha Ray^{1, 2*}

¹*DST-CSIR National Centre for Nanostructured Materials, Council for Scientific and Industrial Research, Pretoria 0001, South Africa*

²*Department of Applied Chemistry, University of Johannesburg, Doorfontein 2028, Johannesburg, South Africa*

*Corresponding author. rsuprakas@csir.co.za; ssinharay@uj.ac.za

This article critically reviews the detailed fundamental understanding of the influence of conductive nanoparticle migration on the localization, and hence, electrical conductivity of immiscible polymer blend nanocomposites. Three types of conductive nanoparticles, namely, spherical, tubular, and platelet, are discussed with respect to their migration and electrical conductivity of obtained nanocomposites. A complete migration process consists of bulk migration within one component, contact with the interface, and penetration to the other component. During processing, the wetting coefficient parameter is the main thermodynamically controlling factor for nanoparticle localization. However, kinetic effects, such as mixing sequence and intensity, viscosity ratio, size and shape of the nanoparticles, and mixing time, can play a substantial role in determining the final locations of nanoparticles. Moreover, the rate of migration varies with the surface chemistry of the nanoparticles. It has been reported that nanoparticles in a more viscous phase move slower compared with a low viscous phase. Furthermore, nanoparticles having high aspect ratios and surface polarities compatible with the other component migrate faster. It is established that immiscible polymer blend nanocomposites with a “double percolation” structure having higher conductivity with nanoparticles localized at the interface of the co-continuous blends.

Keywords. Polymer blends; nanoparticles; migration; interface; percolation; conductivity.

1. Introduction

The incorporation of nanoparticles into polymeric materials has attracted phenomenal attention over the last two decades owing to their unique characteristics in delivering remarkable improvements in electrical conductivity, and mechanical, thermal, barrier, fire retardance, and other material properties^[1-4]. In this direction, electrically conductive polymer nanocomposites have attracted a great deal of attention in diverse applications such as in electromagnetic interference shielding (EMI)^[5, 6], conductors^[7, 8], anti-static materials^[9], sensors^[10] and in flexible electronics^[11] owing to their lower costs and weight, more flexibility and resistance to chemical corrosions in comparison with metals. Recently, carbon-based conductive nanofillers have been extensively used in immiscible polymer blends due to the role that they can play in reinforcing properties with respect to the desired application^[12]. Immiscible polymer blends mean that from a thermodynamic point of view, the Gibbs free energy change of the system is positive ($\Delta G_{mix} > 0$)^[13]. Thus, immiscible polymer blends yields a phase-separated-structured with characteristics intermediate between those of each constituent, which can vary depending on the final morphology of the blend. Therefore, nanoparticles have been incorporated to immiscible polymer blends to stabilize morphology and produce uniform structures with enhanced mechanical properties and electrical conductivity. Many research articles are devoted to defending the compatibilization effects of nanoparticles of different shapes such as platelets like graphenes^[14-20], spherical-shaped particles like carbon black (CB) particles^[21-23], and tubular fillers such as carbon nanotubes (CNTs)^[24-26]. In short, nanoparticles can contribute to morphology stabilization by increasing the interfacial adhesion between two polymers when they are localized at the interface or by changing the viscosity ratio of the blend when accumulated in one of the phases. Suppressed coalescence due to steric repulsion is the major reason behind the size reduction mechanism when nanoparticles are localized at the interface between matrix and dispersed phase droplets^[27]. In the latter case, when nanoparticles are accommodated inside the polymer matrix, the breakup process of dispersed phase droplets is facilitated during processing. Hence, knowing the nanoparticle localization would help us understand the compatibilization process, and in turn, the best choice of nanoparticles for a blend system. Taguet et al.^[28], in a review article, summarized the thermodynamic theories discussing phase separations in filled blend systems and the different compatibilization mechanisms that nanoparticles can cause in polymer blends. In another interesting article, Bose et al.^[29] viewed the filled blend system from a different perspective when concluding that utilizing a blend system as opposed to the single phase polymer can facilitate the dispersion of multiwalled CNTs (MWNTs) in a poly[(α -methyl styrene)-co-acrylonitrile]/poly(methyl methacrylate) (P α MSAN/PMMA) blend. This point of view is the

rationale behind the optimized conductivity in polymer blends with low electrical percolation thresholds, which will be discussed in this article. Electrical percolation threshold is considered to be the concentration that shows the most remarkable electrical conductivity improvement below which the conductivity is negligible. Generally, from the literature, it can be said that the role of nanoparticles in stabilizing immiscible blends is inevitable; however, care must be taken during the processing stage to optimize the nanoparticles distribution regarding their localization with respect to the targeted final properties, namely electrical conductivity. This includes the migration of nanoparticles within the blend system from one component to the other one during processing (mixing) or post-processing (annealing) both at the melt-state.

The current review critically discusses fundamental understanding on how this unique migration phenomenon can affect the nanoparticle's final localization and consequently the conductivity of the polymer blend nanocomposite. Moreover, the thermodynamic distribution of nanoparticles at equilibrium is explained using the wetting coefficient parameter (ω_{AB}) and the proposed mechanisms behind the migration process are summarized. The different factors from the processing level (e.g., shearing forces, mixing protocol, and time) to material-related (e.g., viscosity ratio, particle size, and nature), bringing forth perturbation of the equilibrium state and causing the migration of particles to happen are reviewed in the context of available information. Finally, we focus on how the migration of nanoparticle can be utilized to tune the electrical conductivities of immiscible polymer blend nanocomposites with respect to their corresponding morphologies, considering that an effective conductive network can be formed by localizing nanoparticles at the interface of a co-continuous blend.

2. Particle Localization in the Equilibrium State

Final morphologies, and consequently, properties of the blends are highly dependent on the localization of the particles within the polymer blends. Hence, the knowledge of particle distribution inside the blends can help manufacturers and researchers to design products aligned to the desired end-use application. Particle localization in polymer blends can be predicted by calculating the wetting coefficient ω_{AB} based on Young's equation (Eq.1), proposed by Sumita et al. ^[30] as follows ^[31]:

$$\omega_{12} = \frac{\gamma_{P-B} - \gamma_{P-A}}{\gamma_{AB}} \quad (1)$$

where γ_{P-A} and γ_{P-B} represent the interfacial tensions between the particle and polymer A and B, respectively, and γ_{AB} is the interfacial tension between polymer A and B. If $\omega_{AB} > 1$, nanoparticles are expected to localize in polymer A and if $\omega_{AB} < -1$ nanoparticles are expected to accumulate in

polymer B; when $-1 < \omega_{AB} < 1$ nanoparticles are expected to be at the interface between polymers A and B. Different methods can be applied to determine the interfacial tensions experimentally and theoretically^[32, 33]. The most commonly used theoretical methods are based on geometric (Eq. 2) and harmonic mean (Eq. 3) equations proposed by Owens and Wendt^[33] and Wu^[31], respectively:

$$\gamma_{12} = \gamma_1 + \gamma_2 - 2 \left(\sqrt{\gamma_1^d \gamma_2^d} - \sqrt{\gamma_1^p \gamma_2^p} \right) \quad (2)$$

$$\gamma_{12} = \gamma_1 + \gamma_2 - 4 \left[\frac{\gamma_1^d \gamma_2^d}{\gamma_1^d + \gamma_2^d} + \frac{\gamma_1^p \gamma_2^p}{\gamma_1^p + \gamma_2^p} \right] \quad (3)$$

where d and p respectively represent the dispersive and polar contributions to the surface tensions of components 1 and 2. Some of the predicted studies are summarized in section 6.4. It has been stated that the geometric mean method is more accurate for high surface energy materials and the harmonic mean approach is more suitable for low surface energy materials^[31].

Estimation of nanoparticle localization using this method seems promising when the equilibrium state is met. However, observing discrepancies between experimental approaches and theoretical predictions is inevitable since these calculations are based on thermodynamic equilibrium wetting conditions, while kinetic and processing conditions can play a crucial role in the final localization of nanoparticles by altering the thermodynamic equilibrium in the melt-state and inducing the migration of nanoparticles. Contrary to the interfacial tension calculation of polymer pairs according to the aforementioned equations (Eq. 2-3), the interfacial tension measurements between polymers and nanoparticles cannot be readily obtained since the values can significantly vary depending on the surface structure of the nanoparticles^[34-37]. It must be noted that surface energies at high temperatures are extrapolated from lower temperatures while the values for solid and melt polymers could be different. Therefore, kinetic effects and processing conditions must be considered when determining the localization of nanoparticles in immiscible polymer blend-based nanocomposites.

3. Migration Mechanisms

Migration of nanoparticles consists of traveling through one component to the other where they meet the interface and eventually penetrate the opposite component. This time-consuming process requires diffusion through the bulk, driving forces such as thermodynamic effects, and adequate hydrodynamic stress. Elias et al.^[38] discussed the three possible mechanisms for a nanoparticle to migrate from one phase to the other as follows:

The *first mechanism* involves diffusion through the Brownian motion of nanoparticles, which is strongly dependent on size and viscosity. **Table 1**^[2, 39] shows the rotary diffusion coefficients of particles with different shapes (L/D aspect ratio), where K_B , T , and η_s are the

Boltzmann constant, temperature, and viscosity, respectively. Thus, the required time (t_D) for a nanoparticle to travel a distance equal to its diameter can be calculated using the equation (Eq. 4) below:

$$t_D = \frac{d^2}{4D_{ro}} \quad (4)$$

Where d is the diameter of a particle and D_{ro} is its rotary diffusion with respect to its shape and aspect ratio. t_D was found to be quite large and incomparable with the situation where shear is applied. Lee et al. [40] found t_D to be 2.57×10^4 s for CNTs to diffuse $1 \mu\text{m}^2$ in a polystyrene/poly(phenylene ether) (PS/PPE) blend under no-shearing conditions. Recently, Bai et al. [37] revealed that it takes 1 h of annealing at 180°C for reduced graphene oxide (r-GO) to diffuse only 50 nm in highly viscous poly(lactic acid) (PLA) under Brownian motion. Therefore, it can be said that the diffusion of nanoparticles to the other phase under Brownian effects is negligible if the t_D of nanoparticles due to convectional motions from the applied force is shorter than this diffusion time, as the high viscosity of the molten polymer hinders such motions. In other words, particle migrations in the highly viscous polymers are non-Brownian where the diffusion coefficient of the nanoparticle is quite low.

Table 1. Rotary diffusivity of particles with different shapes (aspect ratio L/D) [2, 39].

Aspect Ratio (L/D)	Rotary Diffusivity D_{ro} [s^{-1}]
Nearly spherical shape ($L/D \approx 1$)	$D_{ro} = \frac{K_B T}{\pi \eta_s D^3}$ (5)
Platelet-like particle ($L/D < 1$)	$D_{ro} = \frac{3K_B T}{4\eta_s D^3}$ (6)
Prolate spheroids ($L/D > 1$)	$D_{ro} = \frac{3K_B T [\ln 2(L/D) - 0.5]}{\pi \eta_s L^3}$ (7)
Fibers, Rods ($L/D \gg 1$)	$D_{ro} = \frac{3K_B T [\ln(L/D) - 0.8]}{\pi \eta_s L^3}$ (8)

However, Yoon et al. [41] proved that with proper annealing time and having temperature as the main driving force, diffusion can occur with the Brownian motion. In their proposed method, two sheets of polypropylene (PP)/CNT composite and neat polycarbonate (PC) were placed on top of each other (as illustrated in **Figure 1**) and then annealed at 200°C and 300°C . It was found that some of the CNTs can migrate to the PC phase via the diffusion mechanism.

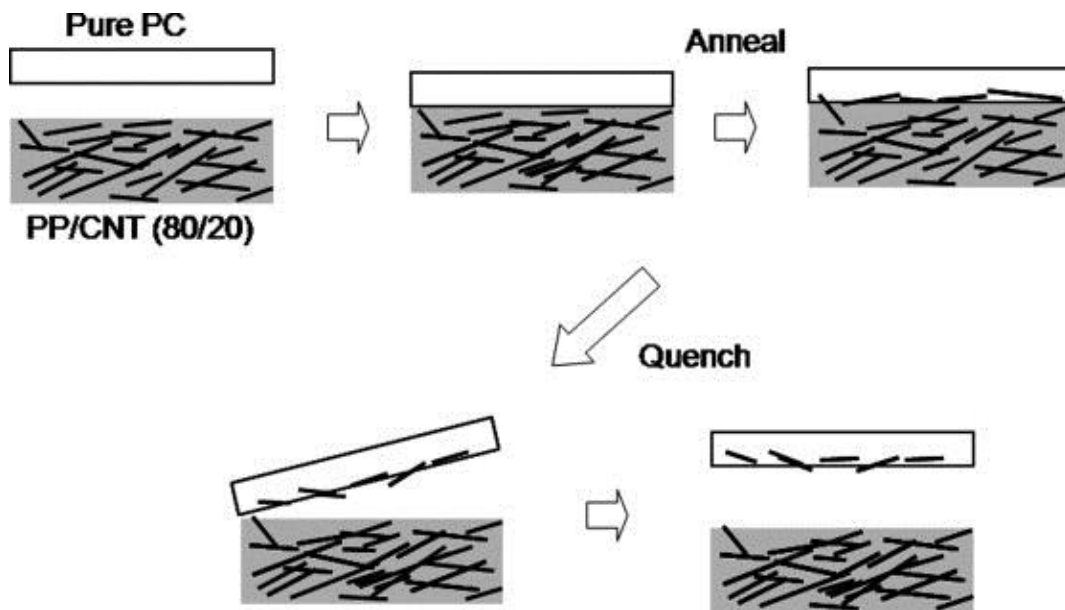


Figure 1. Procedure for depositing CNTs on a PC surface by placing sheets of PP/CNT and neat PC on top of each other and annealing them at different temperatures and time (2, 5, 10, and 20 min). Sheets were peeled off after quenching ^[41]. Copyright 2009. Reproduced with permission from Elsevier Sci. Ltd.

Although it has been cited that such nanoparticle movements are thermally induced; some sort of compatibility is required for Brownian motion to happen ^[2, 41]. Doan et al. ^[42] observed that silica particles will not migrate from poly(butadiene) rubber (BR)/silica to poly(styrene-*co*-butadiene) rubber SBR sheets while they moved from SBR/silica to BR sheets during annealing, indicating that there was some affinity between silica nanoparticles and BR which favored the migration, whereas at higher temperatures migration occurred faster. In other words, surface tension was the first order driving force for migration where silica nanoparticles moved to the phase where the lowest interfacial tension was obtained. Recently, Wiwattananukul et al. ^[43] reported interesting results where they found MWNTs could migrate to PE from PC/MWNT phase during melt blending in a mixer, in contrast with the results of laminated sheets where MWNTs migrated from the PE/MWNT to PC sheets. Although the exact mechanism was not clear, oxygen on the surface of MWNTs was found to be a key parameter during the mixing favoring the interactions in the blend toward the migration to PE. From above discussion we can say that the migration mechanism in the blend is quite different, and diffusion of particles upon only annealing from one phase to another is unlikely to occur.

Shear-induced migration is the *second proposed mechanism* ^[44, 45]. As mentioned earlier the movement of nanoparticles inside a molten polymer is rather translational than Brownian where this boundary is governed by the Peclet number ($Pe \equiv \frac{\dot{\gamma}}{D_{ro}} \propto \dot{\gamma} \cdot t_D$), where $\dot{\gamma}$ is the shear

rate indicating the significant role of shear force on the migration of nanoparticles. When migration in the blend is the concern of the study, random collision of the minor phase droplets can take part in the migration process. During mixing, the floating particles and the second component in the polymer blend can collide frequently and these collisions may result in nanoparticles embedded in droplets. A similar mechanism could be applied when nanoparticles are initially inside dispersed-phase droplets and need to migrate to the interface, and eventually to the polymer matrix due to the velocity field inside the droplets.

The *third mechanism*, which could be not beneficial in terms of morphology stabilization, is when nanoparticles are trapped between two colliding droplets. This mechanism however, could be considered as a special case of previous mechanism as shear forces are also involved. In this case, particles can promote coalescence and end up embedded inside the newly created large droplets. This phenomenon is known as the “bridging-dewetting” mechanism ^[46-50] where nanoparticles are simultaneously absorbed onto the surfaces of two approaching droplets, promoting coalescence if the interface is not completely covered by the nanoparticles, as illustrated in **Figure 2**. The latter case is not a favorable mechanism in blend stabilization where finer morphologies are required.

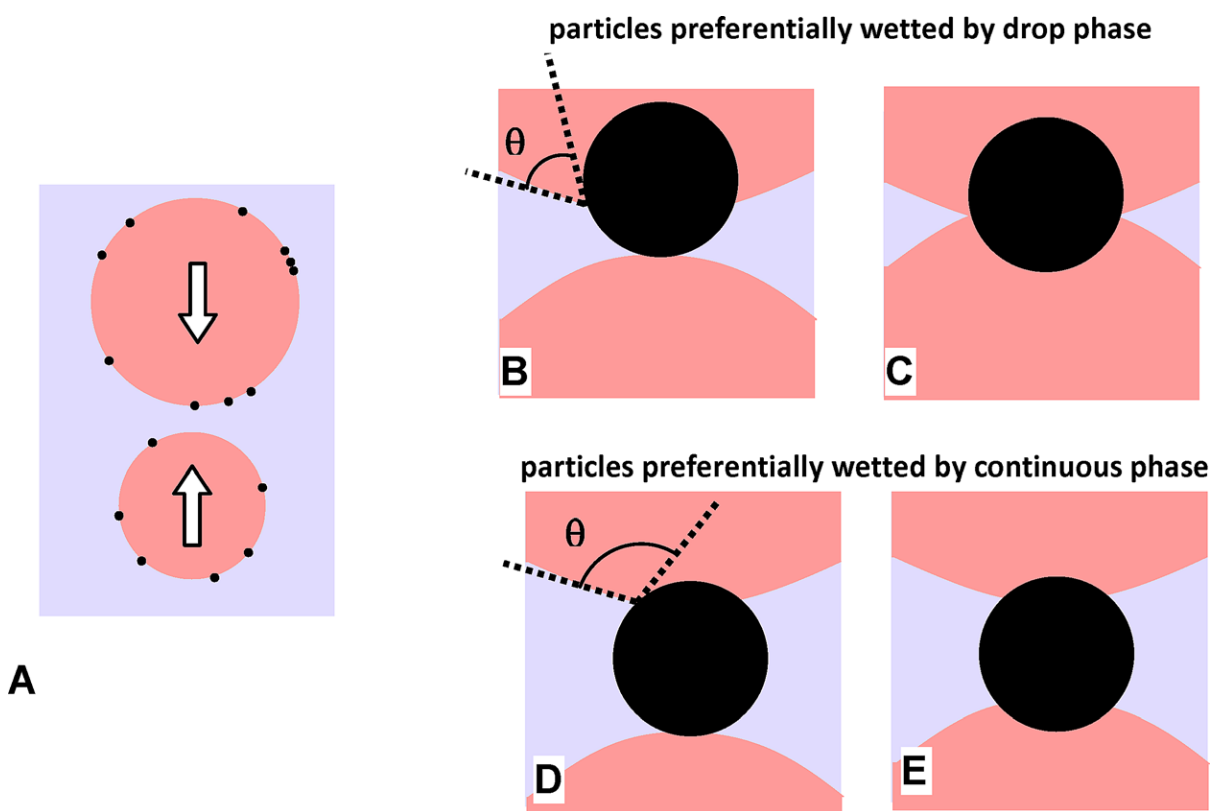


Figure 2. (A) Approach of two droplets with particles on their surfaces. (B) $\theta < 90^\circ$ when particles are wetted by droplets. (C) Coalescence occurs. (D) $\theta > 90^\circ$ when particles are wetted by the

continuous phase. (E) Bridging occurs ^[47]. Copyright 2013. Reproduced with permission from The Society of Rheology.

The mechanisms discussed above can explain some of the possible ways of nanoparticle migrations in an immiscible polymer blend. However, it must be noted that the first mechanism where migration of nanoparticles under static conditions is discussed cannot practically be considered as a migration mechanism in the immiscible blends since the very important governing factor, namely hydrodynamic forces, is required for a particle to travel relatively large distances and penetrate the other phase. In a sense, the other two mechanisms seem more promising describing the possible routes of nanoparticle migration inside an immiscible polymer blend. However, the chemistry point of view of the matter is not discussed where migration seems to be more than just random movement of particles from one phase to another. That is, interfacial energy between nanoparticles and components play a big role in the rate and direction of the migration. Speaking of migration mechanisms of nanoparticles, one must consider the orientation of the non-spherical nanoparticles toward the direction of the migration and eventually the other phase. Gödel et al. ^[51] have discussed the matter which will be explained in detail in section 5.3., where it has been stated that anisotropic nanoparticles (CNTs, clays or graphene-based sheets) perpendicular to the interface of other component would penetrate faster due to curvature instabilities at the interface.

Finally yet importantly, confined free volume-induced migration at high nanoparticle concentration could also be included in the list as another mechanism. This type of migration occurs when enough space is not provided for the desired phase to accommodate the nanoparticles, hence they are pushed out to migrate to the other phase ^[52].

Therefore, the aforementioned arguments enlighten us to the fact that nanoparticles can move to the desired location if conditions are fulfilled. Note that and there could be other external factors governing the final distribution of nanoparticles, such as the magnitude of imposed shear, viscosity ratio, mixing time, the surface nature of nanoparticles themselves, and the nanoparticle geometry, each of which can perturb the equilibrium thermodynamic effects and determine the final location of the nanoparticles. In the next section, we will discuss how these governing factors influence the migration of nanoparticles during mixing in the melt-state.

4. Effects of Mixing Conditions (Dynamic Process)

4.1. Mixing Protocol (or Sequence)

Changing the sequence of mixing of polymer pairs in blending can vary the final localization of the nanoparticles within an immiscible polymer blend ^[53-60]. Given that enough stress is supplied for the affine motion of the nanoparticles in a molten polymer and the fact that

requisite wetting parameters exist for such motions to occur; the order of nanoparticle addition into the blend can interfere with the final localization. Four different possible sequences can be considered if investigating the order of mixing the components. (i) Simultaneous mixing, where all the components are concurrently added to the mixer. (ii) The addition of nanoparticles to the molten blend, where polymer pairs are already mixed for sometimes when the nanoparticles are added. (iii) Premixing with a component that is thermodynamic preferred. (iv) Premixing with a component that is thermodynamic not preferred.

Depending on the sought properties and end-use applications, nanoparticles of different shapes have been incorporated to the immiscible polymer blends. In this section, the effect of the mixing sequence on the final localization of most extensively used conducting nanoparticles, namely carbon black, CNTs, and graphene, will be discussed. The extensive studies (discussed later) on the blending sequence will address that the sequence of mixing can affect the final blend morphology and nanoparticle migration could be the key role player. Premixing nanoparticles inside the phase with the least compatibility can act as a stimulant for the migration of nanoparticles to the other phase with better affinity. That is, thermodynamics can govern the nanoparticle transfers. Therefore, nanoparticles are mostly surface modified to facilitate this thermodynamically driven transfer. It is of importance to select the proper modified nanoparticle with respect to the blend choice. Thus, techniques, such as contact angle measurements^[61, 62], are used to understand the surface energies between components. Eventually, this nanoparticle migration can assist to control the morphology of the final blend especially when they are located at the interface where finer morphology develops. Therefore, if specific morphology is required for a particular application we have to understand what type of surface modification with respect to the premixed polymers polarity and which mixing sequence should be used. Moreover, not only localization but also the degree of dispersion at the final stage of the blend can be controlled with the use of sequential blending where nanoparticles were shown to be dispersed better when they were migrated to the other phase during blending. At last, a sufficiently applied stress is required to initiate the migration that will be discussed in the next section.

4.1.1. Carbon Black

Carbon black (CB), which is one of the most common classic nanofillers in immiscible polymer blends, has been extensively studied due to its reasonable conductivity and reinforcing properties as well as heat and chemical resistance^[63]. Tchoudakov et al.^[64] prepared PP/PA blends filled with different concentrations of CB in three different sequences (see **Table 5**). CB particles were found to be in the PA after melt blending, regardless of the blending sequence. This indicates that CB particles migrated from the less thermodynamically favorable component (PP) to

the more thermodynamically favorable component (PA) during blending when they were premixed in PP. It was found that this migration is a thermodynamically driven process, as it occurred fast during the blending of (PP/CB) +PA. The influence of the blending sequence on the final localization of CB particles in PS/PMMA (volume ratio of 1) blends was investigated by Scherzer et al. [65]. It was found that CB particles would locate in the PS regardless of the mixing sequence. This indicated that CB particles migrated from PMMA/CB to the PS during blending with PS. Migration of CB from one component to the other is reported in other studies as well [66-68]. It was shown that CBs can be frozen at the interface during the migration of CBs from a pre-mixture of PS/CB to the PE phase since CB with nonpolar surface tend to move to the less polar PE [66, 69]. Slit-die extrusion-hot stretching is another procedure proposed by researchers to prepare blends with *in situ* microfibrillar structure [67, 68, 70, 71]. In this particular method, particles were premixed with one of the components prior to blending with other polymer during the next step. For the blending process, the temperature was set in a manner that enabled the melting and flowing of the both components, led to formation of microfibrils. Microfibrils were produced through the slit die when the extrudate was stretched and quenched. The goal was to produce blends with interconnected *in situ* microfibrillar structures to obtain low percolation threshold and having optimized conductivity by locating the nanoparticles at the interface. These studies revealed that to have better interconnection between the microfibrils, particles are needed to be located at the interface. CB particles could migrate to the interface and on the surface of the microfibrils at high particle concentrations (18 vol.%) in a (polyethylene terephthalate/PE) PET/PE (volume ratio of 1:3.2) blend due to high packing concentrations within one component when they were premixed with the favored component PET [68] or due to thermodynamic effects when they were premixed with the disfavored polymer PE [71] (more preferred procedure).

4.1.2. CNTs

Another category of interesting nanofillers that has drawn a great deal of attention is that of CNTs, due to their high aspect ratio (L/D) rendering superior diverse characteristics such as sensing [72-74], mechanical [75, 76], electrical [77-80] and thermal properties [81, 82]. CNTs are basically graphene sheets rolled-up into cylindrical single-walled (SWNT) or multi-walled (MWNT) structures [83, 84]. Their application in polymer blends as interfacial stabilizers and the improvements they bring about in electrical conductivities of the blends at very low percolation thresholds (~0.05 wt. %) have also been reported [24, 85-87].

Gödel et al. [88] studied the influence of the incorporation sequence of MWNTs to co-continuous PC/poly(styrene-co-acrylonitrile) (SAN) blends. TEM results revealed that MWNTs localize in the more compatible phase (PC) irrespective of the incorporation method, indicating the

thermodynamic-driven migration process of the nanotubes toward the PC phase. This was in accordance with theoretical calculations based on the wetting coefficient parameter. Baudouin et al. [34] observed the migration process of MWNTs in (90/10) ethylene acrylate (EA)/PA12(PA6) blends. It was shown that when nanotubes were premixed with PA they remained inside the PA phase with some migrating to the interface; however, in the case of PA12, all the MWNTs were dispersed well inside the PA phase. On the other hand, when MWNTs were premixed with the EA, most of the nanotubes were found at the interface after blending with PA and some were able to enter the PA12 after blending, indicating more affinity of MWNTs toward PA12. Finally, when all components were mixed simultaneously, nanotubes were found at the interface and some in the PA (in the case of PA12). Interestingly, the morphologies were stable after 60 min of mixing indicating that thermodynamics dominated the final partitioning of nanotubes. **Figures 3 and 4** show schematic views of the migration mechanism involved for the three mentioned sequences when PA6 and PA12 were used, respectively.

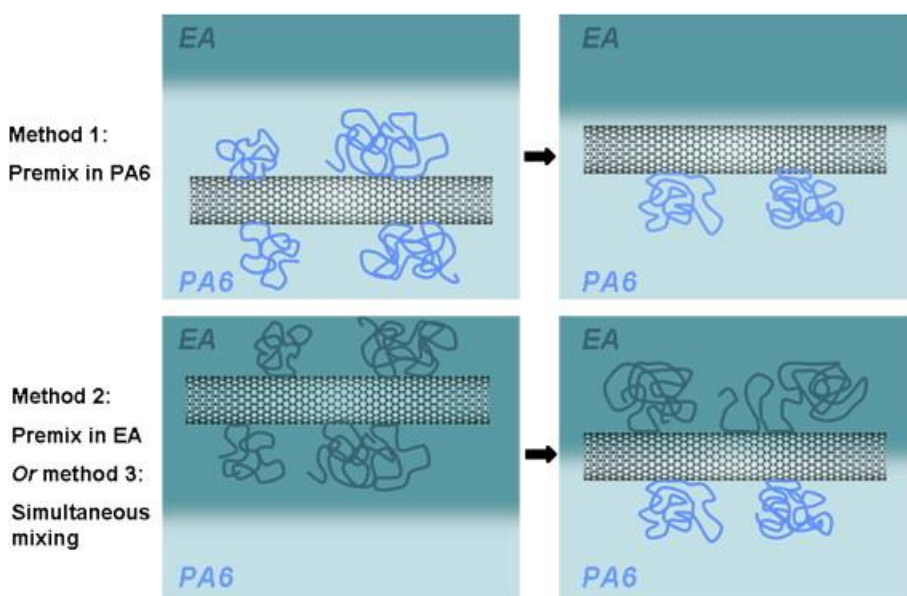


Figure 3. Schematic view of migration mechanism of MWNTs in EA/PA6 with respect to their mixing sequence [34]. Copyright 2010. Reproduced with permission from Elsevier Sci. Ltd.

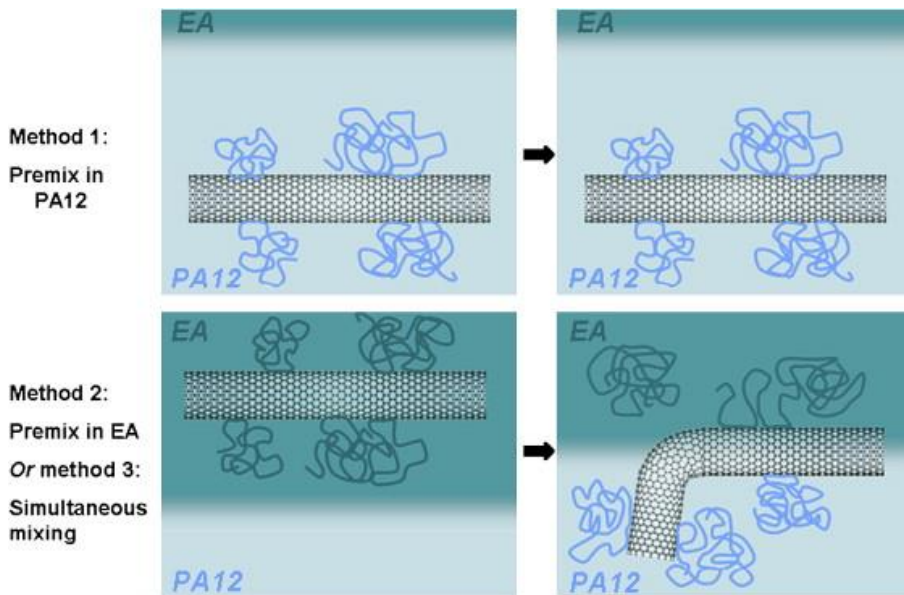


Figure 4. Schematic view of migration mechanism of MWNTs in EA/PA12 with respect to their mixing sequence^[34]. Copyright 2010. Reproduced with permission from Elsevier Sci. Ltd.

The same authors^[89] examined the localization of MWNTs in a copolyamide 6/12/ (ethylene-acrylate copolymer) (PA6/12)/EMA blend where PA was a copolymer of PA6 and PA12. PA was the minor phase in all prepared blends with different protocols. It was shown that most of the MWNTs were located at the interface when they were premixed with the EMA or when simultaneously mixed while they remained inside the PA when premixed with PA, indicating the higher affinity of MWNTs toward the PA phase. Similar results were reported by Zonder et al.^[26] in PA/PE/CNT blends. It was revealed that CNTs migrated to the interface when they were pre-dispersed in the PE phase or mixed simultaneously while they remained inside the PA phase when they were pre-dispersed in the PA phase.

Xu et al.^[90] prepared (polyphenylene sulfide/polyamide 6)/MWNT (PPS/PA6/MWNT) nanocomposites in a similar fashion where MWNTs were pre-compounded with the unfavorable PPS matrix. The results revealed nanocomposites with MWNT particles located at the interface or in the PA6 phase, indicating the migration of MWNT from PPS to PA6. It was reported that the nanocomposites prepared via this method were capable of forming networks whereas the single-step method was unable to result in such nanocomposites due to the isolation of MWNTs inside the PA6 when the PA6 was the minor component (20 wt. %). In another study^[91], it was found that CNTs tended to migrate toward the EVA phase from PLLA in nanocomposites prepared via a PLLA/CNT masterbatch and remained inside EVA when prepared via an EVA/CNT masterbatch, despite the fact that predictions based on the surface energies revealed higher affinity of CNTs toward PLLA (**Figure 5**).

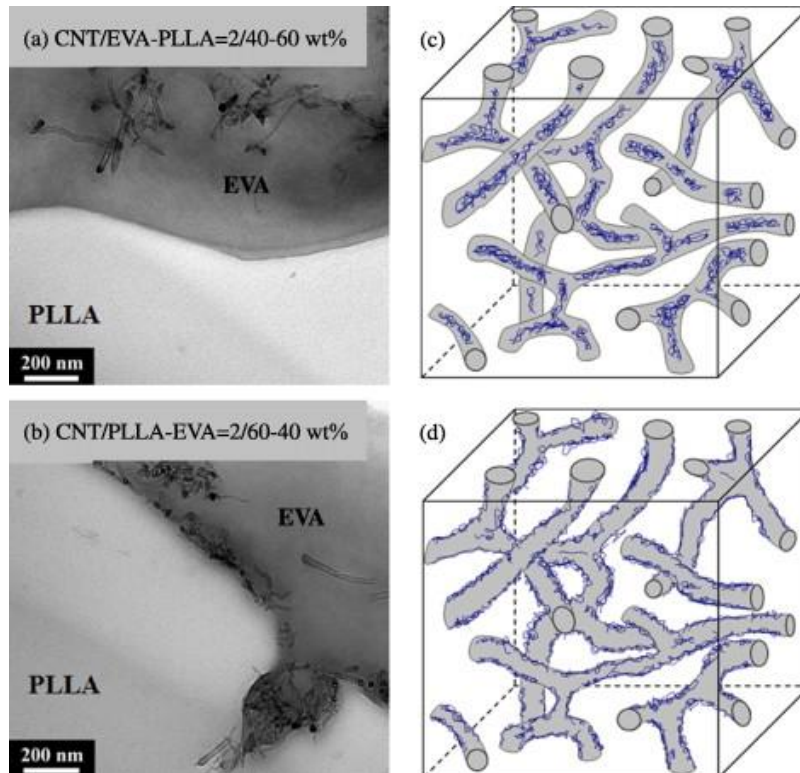


Figure 5. CNT localization in PLLA/EVA/CNT nanocomposites prepared via (a) CNT/EVA masterbatch and (b) CNT/PLLA masterbatch methods ^[91]. Copyright 2013. Reproduced with permission from Elsevier Sci. Ltd.

Pötschke et al.^[92] utilized the dilution method where concentrated PE/MWNT composites were blended with PC or PA6. During the melt-blending dilution process, almost all of MWNTs migrated to the PA6 or PC due to more favorable interactions between the MWNT and the PA6 or PC. This led to the formation of composites with excellent dispersion of MWNTs without agglomerations. Similarly, Lee et al. ^[40] revealed that CNT migrated from a (polystyrene/poly phenylene ether/CNT) (PS/PPE)/CNT masterbatch to the more favorable PA66 phase after blending in a (60/40) PA66/(PS/PPE) blend. This resulted in a better dispersion of CNTs in the PA66 phase relative to the other sequences where CNTs were initially premixed with PA66 or added simultaneously. The authors proposed the term “filler-transfer-induced dispersion” to explain this phenomenon, as shown in **Figure 6**. It was suggested that nanotubes migrated to the PA66 phase in a two-step mechanism where they first met the interface due to shear-induced collisions and then transferred to the PA66 phase as a result of instabilities in interfacial curvature. In other words, the migration process assisted in yielding blends with better dispersion of CNTs in the PA66 phase.

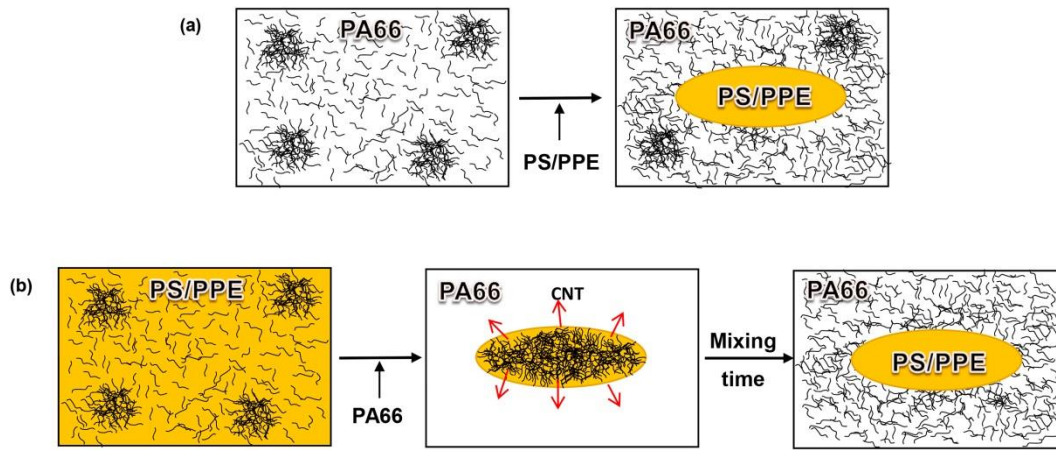


Figure 6. Illustration of CNT dispersion. (a) Nanocomposite prepared according to compounding sequence II, and (b) CNT dispersion by “filler-transfer-induced dispersion” in nanocomposite prepared according to compounding sequence III ^[40]. Copyright 2016. Reproduced with permission from Elsevier Sci. Ltd.

In a recent study, Gong et al. ^[93] took advantage of a similar migration process to produce a well-dispersed ethylene- α -octene random copolymer (ORC)/MWNT composite. In their work, poly (ethylene oxide) (PEO)/MWNT composites were initially prepared before blending with ORC. A 50/50 PEO/ORC weight ratio was used to ensure having a co-continuous morphology. During melt blending, MWNTs migrated toward the ORC phase due to higher affinity while preserving their isolated structure, and eventually all of the MWNTs migrated to the ORC phase after 15 min of melt blending. After completing the migration, the PEO phase was washed out using deionized water leaving a uniform and homogenous ORC/MWNT composite. A schematic view of the proposed method can be seen in **Figure 7**. It was found that composites prepared via the help of migration were more uniform than those prepared directly using a melt mixing process. The argued results show that altering the blending protocol can affect the localization of CNTs as well as the state of dispersion with respect to the blending order. It was found that dispersing CNTs in a thermodynamically disfavored phase (CNT masterbatch) before blending with the other neat phase could be a promising method to enhance the migration process to place them at the interface or even disperse them in the other phase.

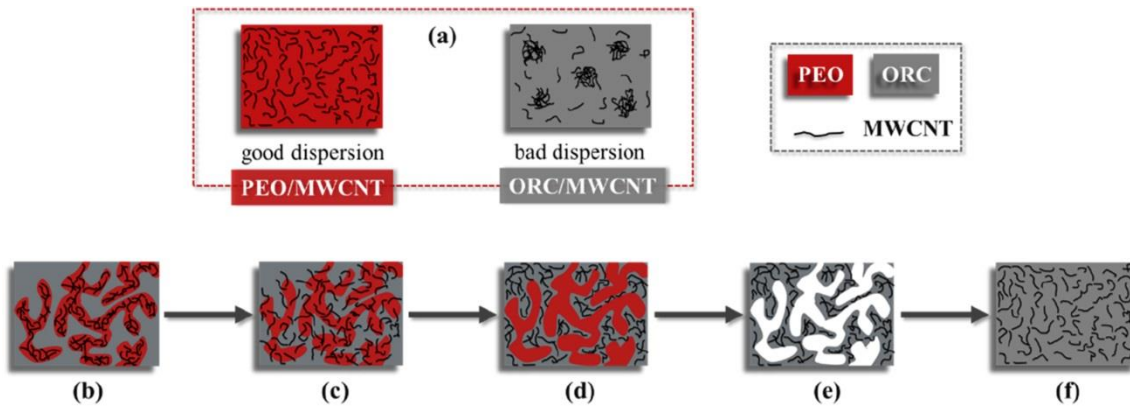


Figure 7. Schematic diagram for improving the dispersion of MWNTs in an ORC matrix. (a) The dispersion of MWNTs in PEO and ORC matrix; (b) uniform dispersion of MWNTs in the PEO phase of PEO/ORC blends; (c) singular migration of MWNT from the PEO phase to the ORC phase; (d) completion of MWNT migration; (e) selective removal of the PEO phase using water; and (f) homogenous dispersion of MWNTs in ORC matrix of R-ORC/MWNT composites obtained by the re-melting process^[93]. The samples with removed PEO named R-ORC. Copyright 2017. Reproduced with permission from Elsevier Sci. Ltd.

4.1.3. Graphene-based particles

Graphene is a new class of two-dimensional planar hexagonal (honeycomb) crystal lattice with extraordinary electronic and mechanical properties^[94-97]. Initially it is noteworthy to address that graphene is referred only to the monolayer of single-atom-thick sheet. However, researchers and manufacturers use different terminologies, which do not comply with the definitions. A very comprehensive article published by Bianco et al.^[98] has elaborated the different definitions. Therefore, we named this subsection as “Graphene-based particles”; however, this article used the definition as it has been reported in each reference. Graphene-based nanofillers have been used in polymer composites^[99-101] and blends^[37, 102-106] due to their unique properties^[107, 108]. Liebscher et al.^[102] studied the effect of processing conditions and mixing sequence on the localization and dispersion of graphene nanoplatelets (GNP) in (59/40/1 wt. %) PC/SAN/GNP blends. It was revealed that graphene nanoplatelets remain inside the PC phase when they were premixed with PC before blending with SAN. On the other hand, they migrated toward the interface and the PC phase depending on the mixing speed and time when they were premixed with the SAN phase before blending with PC. This indicated that graphene platelets have similar thermodynamic characteristics as CNTs and also that their dispersion quality in the premixture can affect the migration process such that mild mixing conditions (short mixing time and lower mixing speed) would lead to dispersion of graphenes in aggregates while mixing at longer times and higher speeds produced better dispersions. That is, well-dispersed graphenes could migrate more efficiently toward the more favored PC phase. Paydayesh et al.^[109] investigated the localization effect of graphene nanoplatelets (GNPs) and graphene oxides (GOs) on the morphologies of

(40/60) PLA/PMMA blends. In the case of GNP-filled blends, nanoplatelets mostly occupied the PMMA phase due to their better affinity toward the PMMA phase. This indicates that GNPs had to migrate from the PLA phase to the PMMA phase when they were initially premixed with PLA. On the other hand, GO was found to be in the phase where it was initially premixed and only some small migration to the interface was observed during two-step mixing. This could also raise the question of the effect of processing strategies on migration and localization of the particles in the latter case. Cao et al.^[104] used a two-step process to fabricate (90/10) (PA/polyphenylene oxide) PA/PPO blend with 0.5 wt.% of graphene oxide sheets (GOSs). First masterbatch of PPO/GOS was made through a solvent blending procedure, and then the masterbatch was melt blended with PA in a Haake mixer. It was found that during the melt-blending the GOSs migrated to the interface due to the formation of hydrogen bonds with PA. This in turn enhanced the compatibility of the blend and reduced the interfacial tension. In a recent study, Kelnar et al.^[110] investigated the effect of GO and alkyl modified GO on the properties of (95/5) PA6/ethene-propene elastomer (EPR) blend. They found that when GO was premixed with EPR they could migrate towards PA matrix and interface, hence contributed to the size reduction. On the other hand, the modified GO remained inside the rubber inclusions due to its better affinity and led to the formation of rougher morphologies with lower toughness than unmodified GO incorporated blend.

4.2. *Mixing protocol-(time)*

When dynamics of a kinetically controlled phenomenon is being studied, one cannot exclude time. That is, given that requisite thermodynamic and other kinetic conditions (e.g., viscosity ratio, shear stress, etc.) are already sufficient for a nanoparticle's relocation inside a particular immiscible blend the migration process is a matter of time. In sequential blending, the migration of the nanoparticles is a time-dependent process where if a sufficient time is not given the migration may not occur or may happen inefficiently. Therefore, it will be helpful if the migration rate is observed over time to gain a clearer understanding of the degree of nanoparticle transfer. This relocation depends on the viscosity of the medium where at higher viscosities nanoparticles move slower (See section 5.3).

Göldel et al.^[111] investigated the kinetics of CNT migration through the interfaces in SAN/PC blends. Because CNTs have higher affinity toward the PC phase, they were embedded in the SAN phase during the premixing procedure to observe the migration process during melt blending with the PC phase at 10, 30, and 60 s in a kneading chamber. It was found that no CNT-free phase could be observed at 30 s, indicating that 30 s is when the most migration occurs. Moreover, it was revealed that collision-induced migration during morphology development is the main driving force for the CNT transfer from SAN to PC. In contrast, the migration process of

MWNTs from PPS to PA6 in a PPS/PA6/MWNT nanocomposite was found to be a very slow process where it took 16 min for particles to reach the interface and 30 min to accumulate inside the PA6 phase^[90]. Zhao et al.^[112] also reported that the complete migration of MWNTs from PS to PVDF would take more than 30 min. It was suggested that the large viscosity ratio of the blend could be the reason for such a long migration process, as discussed before^[69, 113]. Lee et al.^[40] found that CNTs could migrate to the more favorable PA66 phase when they were initially dispersed in the (PS/PPE) phase before blending with PA66 compared to other sequence when they were already premixed with PA66. They reported that within 30 s of mixing CNTs were still mostly in the (PS/PPE) phase while at the longer mixing time (60 s), CNTs migrated to the PA66 phase and eventually, at 180 s, they were uniformly dispersed in the PA66 phase. This suggests that migration-induced dispersion of CNTs can be utilized to produce nanocomposites with finer dispersions.

From the above-mentioned results it can be deduced that apart from the thermodynamic forces the migration of nanoparticles can be kinetically controlled; the extent of migration and in turn the final properties are also dependent on the mixing time. A short mixing time might end up having fewer nanoparticles in the desired phase. Mixing for too long at some cases might cause complete migration to the minor phase if it is the thermodynamically favored component. Accumulation of high concentration of nanoparticles especially spherical ones inside the droplets in droplet-matrix morphologies could increase the viscosity of the droplets hence the breaking up would be hindered. On the other hand, at a critical concentration of platelet-like nanoparticles as well as blend ratio, platelet-like nanoparticles such as clays, graphite nanoplatelets and graphene oxides could form a “knife-like” structure and cut the host component into smaller pieces through a “cutting effect” mechanism^[110, 114-116]. Another aspect of time-dependent migration is the viscosity of the polymers, meaning that under similar applied stress the migration rate of a particular particle varies for different blend systems due to different viscosities. The effect of viscosity ratios will be discussed separately in section 5.4. At last, more care should be taken when varying time during blending since some materials such as polyamides, Pes, and PLAs are sensitive to degradation (thermal and oxidative) and increasing mixing time could extensively sacrifice their thermal properties in the favor of nanoparticle distributions^[117-119].

4.3. *Effect of shear forces*

As discussed above the migration is a time-dependent process and if it needs to be done for specific distribution in a particular blend, one practical way to accelerate the process is to increase the applied force. At this point, it is useful to begin with the capillary number since we are dealing with shear stress. In an immiscible polymer blend the droplet deformation is controlled by the

balance between viscous (hydrodynamic forces τ) and cohesive forces, (α/R with α as the interfacial tension and R the droplet radius) ^[120, 121]. The ratio of the above mentioned forces can be defined in a single dimensionless number in a simple shear flow named Capillary number (Eq. 9):

$$Ca = \frac{\tau}{\alpha/R} = \frac{\eta_m \dot{\gamma} R}{\alpha} \quad (9)$$

where R is the radius of the droplet at rest, η_m is the polymer matrix viscosity, $\dot{\gamma}$ is the shear rate, and α is the interfacial tension. If the capillary number exceeds the critical number ($Ca \gg Ca_{cr}$) droplets begin to breakup into smaller ones since shear stress overrules the interfacial stress. This critical number can be varied depending on the viscosity ratio ($K = \eta_d/\eta_m$) where droplet breakup is relatively easier when $K < 1$ than the case when $K > 1$ and for situations beyond $K \sim 4$ droplet breakup is unlikely to occur ^[122]. Therefore, it will be crucial to control the nanoparticles localization in the favor of morphology stabilizations. Further, as mentioned in previous sections, nanoparticles and dispersed phase droplets may encounter a large number of collisions during the mixing process, which leads to the shear-induced migration process of nanoparticles towards the more thermodynamically favored component. The frequency of these collisions can be estimated using the following equation ^[38, 123]:

$$C = \frac{8\dot{\gamma}\phi}{\pi} \quad (10)$$

where ϕ is the volume fraction of the dispersed entity (polymer droplet or particle) and $\dot{\gamma}$ is the shear rate. It can be inferred that increasing the shear rate would increase the collision frequency and hence the probability of the migrations. Moreover, apart from the increase in the frequency of collisions, the increase in shear rate can facilitate particle motion owing to the large forces produced by hydrodynamic shear flow ^[44]. Thus, many researchers studied the effects of shear stresses on the extent of nanoparticle migration. Most interesting one from Dharaiya and Jana ^[124], who studied the influence of nanoclay particles on the morphology changes of (90/10) PA6/PP-nanoclay blends during mixing in a batch chaotic mixer. Silicate layers were premixed with PP and then mixed with PA6 to achieve the desired blends. Different morphologies from lamellas and fibrils to droplets were found depending on the extent of applied shear rate. It was shown that when PP is in a lamellar or fibrillar state (lower shear rates), the nanoclay particles were still in the PP phase. Further, when mixing was intensified at higher shear strains, the fibrils broke up into droplets where nanoclay particles migrated to the PA6 phase due to the applied shear rate. The same authors ^[125] reported the effect of CB on the same blend system in a similar manner. It was revealed that at low strains (equivalent to lower mixing times); CBs were in the PP dispersed phase while at higher strains ($\gamma \geq 2662\%$) they were found at the interface (**Figure 8**).

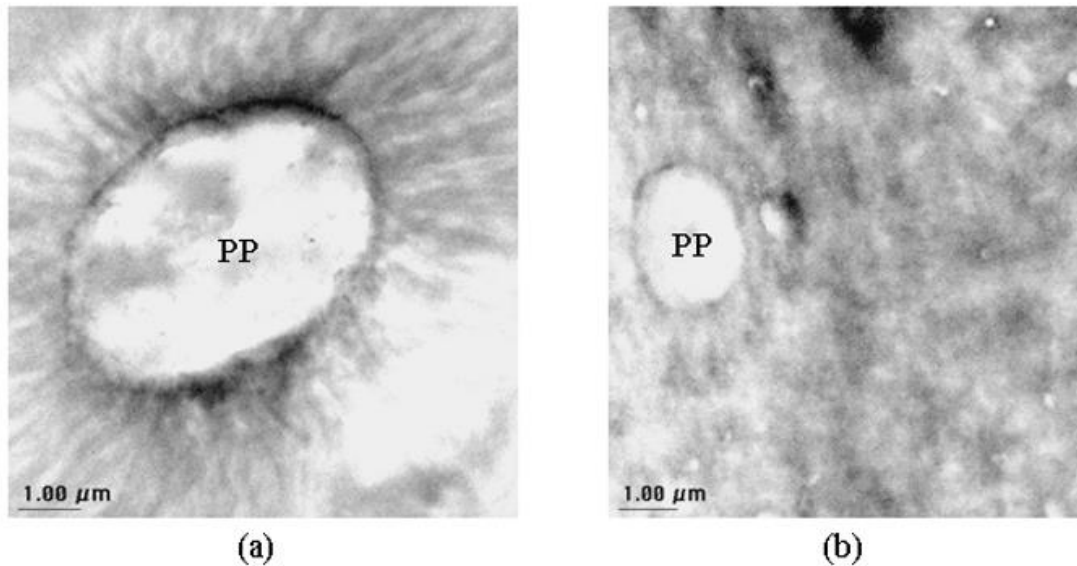


Figure 8. TEM images of PA6/PP/CB blends at (a) strain $\gamma = 1334\%$ and (b) $\gamma = 2662\%$ ^[125]. Copyright 2006. Reproduced with permission from Wiley-VCH Verlag.

This provides evidence of the shear-induced migration of nanoparticles within a blend. In a different study, Li and Shimizu ^[126] reported that when PA6/PVDF/CNT blends were processed at high shear (1000 rpm) during extrusion, some PA6/CNT inclusions were found inside the PVDF phase despite the higher affinity of CNT for PA6. This was not observed for low shear processed (100 rpm) samples indicating that CNT-laden PA6 inclusions migrated to the PVDF phase at high shear rates (See **Figure 22**). Taghizadeh and Favis ^[35] studied the effects of shear fields on the localization of CNTs in (80/20) poly(ϵ -caprolactone)/thermoplastic starch (PCL/TPS) blends. They found that CNTs from a PCL/CNT masterbatch migrated mostly to the TPS phase (and some to the interface) during the twin-screw extrusion process, which was in contrast to the wetting coefficient predictions that estimated the interfacial localization of CNTs. When an internal mixer was used to blend a PCL/CNT masterbatch with TPS, CNTs were found to be located at the interface or remained in the PCL phase, as shown in **Figure 9**. They concluded that higher shear intensities in the twin-screw extruder (100 rpm \approx 88/s apparent shear rate) lowered the TPS viscosities and facilitated the migration of CNTs to the TPS phase compared to the relatively less intense shear fields (100 rpm \approx 52/s apparent shear rate) in an internal mixer (higher viscosity of the TPS hindered the migration of CNTs).

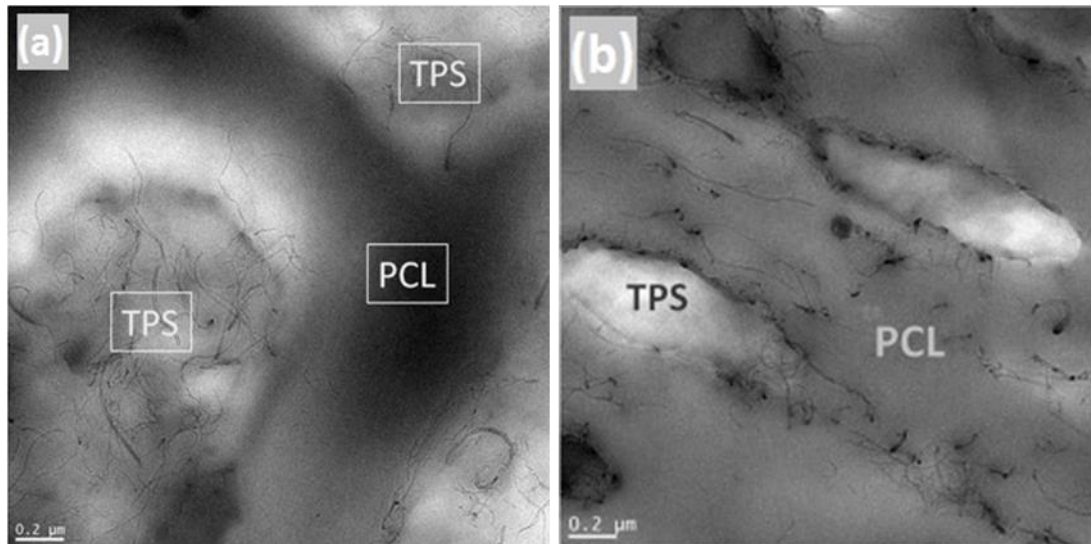


Figure 9. TEM images of (80/20) PCL/TPS blends filled with 2 wt% CNT prepared via (a) twin extruder and (b) internal mixer. CNT was premixed with PCL prior to blend with TPS ^[35]. Copyright 2013. Reproduced with permission from Elsevier Sci. Ltd.

Recently, Jaensson et al. ^[127] employed simulation calculations to study the influence of shear on the migration of a spherical particle in a two-phase fluid system. In their study, the migration was investigated from a viscoelastic fluid (located at the bottom) to a Newtonian fluid (located on top) considering that particle has a tendency to migrate towards the other fluid (on top) due to the gradients in normal stresses. The simulation results revealed four possible scenarios for a particle under shear depending on the magnitude of Weissenberg number ($W_i = \dot{\gamma}t$ where $\dot{\gamma}$ is the shear rate and t is the relaxation time) and capillary number. Table 2 summarizes the different scenarios for a particle depending on the W_i when capillary number is 1. It was shown that at higher $W_i = 3$ particle remained attached to the interface due to the decreased angular velocity.

Table 2. The state of migration from the viscoelastic fluid to the Newtonian fluid when $Ca=1$. The data are generated based on findings from reference. ^[127]

Particle Position	W_i
Moving Away from interface	0
Migration is halted	1
Penetrates to the Newtonian fluid	2
Absorbed at the interface	3

For both higher W_i and Ca numbers particle moved to the Newtonian fluid (upper one). The results implies the important role of shear on the localization of particles in two-phase fluid systems.

5. Effects Associated with Constituents

5.1. Influence of the Wetting Parameters

In section 2, it was discussed how final localization of nanoparticles can be predicted using the wetting coefficient ω_{AB} with respect to the interactions between components reiterating the important role of the interfacial tensions in determining the location of nanoparticles. However, the predictions based on the wetting coefficient could be only considered if the thermodynamic equilibrium is not perturbed by means of processing conditions and kinetics effects. In order to reach the equilibrium state particles may undergo a relocation process if they are not pre-dispersed within the preferred component. Such a process may include the migration of a nanoparticle from one component to another, crossing the interface. That is, a full migration consists of a two stage process, one, from bulk of a component to the interface and second, penetrating the interface.

The required energy for a single spherical nanoparticle with radius r (small enough that external forces such as gravity can be neglected) to travel from a bulk fluid (e.g., water) to the oil/water interface (energy of detachment) can be calculated using the following equation ^[128, 129]:

$$-\Delta G_{\text{int}} = \pi r^2 \gamma_{ow} (1 \pm \cos \theta_{ow})^2 \quad (11)$$

with γ_{ow} as the interfacial tension of the oil/water interface and θ_{ow} the contact angle. It is then shown that this energy for very hydrophilic particles ($\theta \ll 90^\circ$) and very hydrophobic particles ($\theta \gg 90^\circ$) is small, leading the nanoparticles to remain inside either the water or oil phase, respectively. In contrast, for particles with contact angles near 90° , the large interfacial energy of attachment of particles to interface hinders the ejection of particles from the interface ^[130].

Stancik and Fuller ^[131] proposed a model to estimate the maximum adhesive force required to desorb the nanoparticles with R aggregate radius into the oil phase from the interface as follows:

$$F_m = 2\pi^2 \gamma R \cos^2(\theta/2) \quad (12)$$

Many attempts have been made to develop models, determining contact angles of particulate systems; however, the experimental errors cannot be neglected. It is worth noting that the majority of models are based on spherical nanoparticles. The situation where nanoparticles are flake-like, platelets or tubular, the direction on which the nanoparticle is sitting at the interface can remarkably affect the wetting efficiencies and penetration rates. Moreover, interfacial tension calculations between polymer and nanoparticle are complicated task especially at high temperatures since most of the previous measurements were conducted at room temperatures. In addition, existence of surface modified nanoparticles may induce some reaction between polymers

and the nanoparticles. In such cases, wetting coefficient calculation cannot be valid. Furthermore, the additives in most of the commercial polymer products, such as anti-oxidants, UV-stabilizers, etc., can have a significant effect on the surface tensions of the polymers ^[123]. Despite all the effects interfering with the calculations, the importance of surface tensions, in other words interaction between polymer and nanoparticles, stands still. Taguet et al. ^[28] tabulated a list of surface energy, polar and dispersive components of some of the commercially available fillers displaying different ranges of values owing to their surface modifications. This implies the important role of surface functional groups on the surface tensions hence the final localization of the nanoparticles. This in turn can exert differences on the rate of migrations depending on the type of the surface modification.

In a study conducted by Gubbels et al. ^[69], the migration process of CB from one phase to the other was monitored in a (45/55) PE/PS blend. Two different CBs with opposite polarities, each with more affinity toward one of the components (PE or PS), were used to observe the migration of nanoparticles to the other component during melt mixing. At first, CBs were premixed with the non-preferred PE or PS for 3 min, and then the more preferred PE and/or PS was added and mixed for different lengths of time. It was found that CBs migrated to the more favorable polymer (PE and/or PS) by passing through the interface as a function of mixing time due to the existing thermodynamic forces.

Sirisinha and Prayoonchatphan ^[132] studied the effect of filler polarity on the localization of fillers in (BR/NBR) (butadiene rubber/nitrile BR) blends. It was revealed that non-polar CB would locate inside the non-polar BR phase while polar precipitated silica fillers preferentially located inside the polar NBR phase in the (20/80) BR/NBR blend. Although they reported that in the (50/50) BR/NBR blend, the lower viscosity of BR is a factor determining the localization of silica particles rather than silica polarity. In addition, it was shown that increasing the polarity of NBR by using increasing the acrylonitrile content facilitated the migration of non-polar CB to the BR phase.

Liu et al. ^[133] used functionalized MWNT to improve the morphology and consequently the toughness of PP/EVA blends. CNTs were functionalized in such a way that they were more compatible with the EVA phase. It was shown that MWNT had a significant effect on morphology and impact strength due to the double-percolation structure when the blends had a co-continuous morphology (60/40) PP/EVA. On the other hand, it had less influence on the (80/20) PP/EVA blend when the blend showed droplet morphology. It was proposed that at low MWNT content, nanotubes make a single-network structure inside the EVA phase unable to move to the interface or in the PP matrix, hence contributing to interfacial modification. At higher content, some of the self-entangled nanotubes with lengths larger than the EVA droplets stretched toward the other

phase (PP) causing a weak bridge between the phases. This effect is more remarkable in the case where the morphology is co-continuous due to the higher chances of migration of MWNTs at higher content as a result of the larger interfacial areas in this composition. **Figure 10** illustrates a schematic view of the mechanisms of distributing functionalized MWNTs (f-MWNTs) in blends.

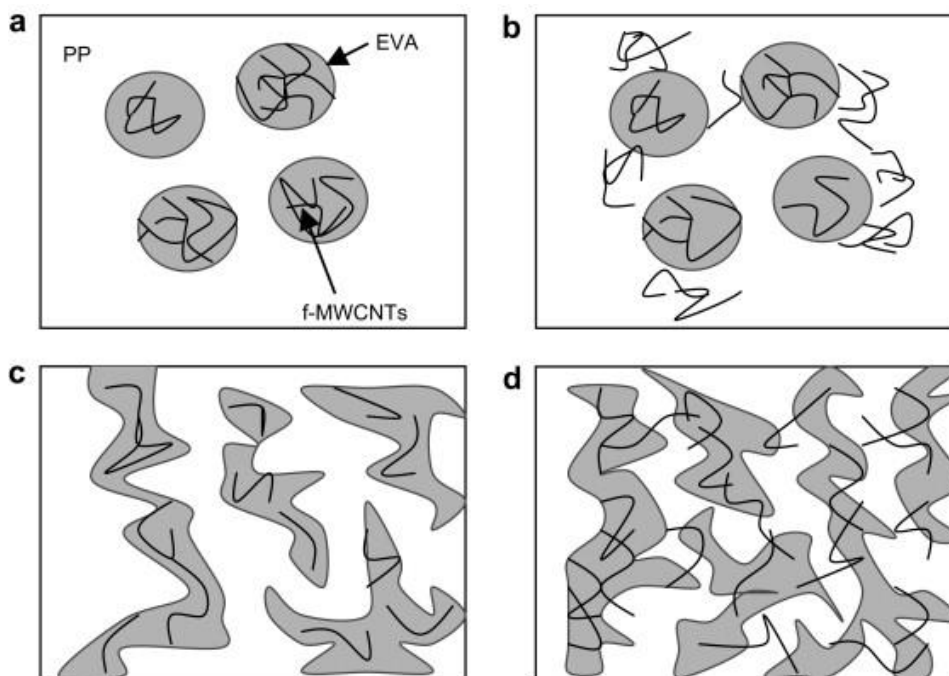


Figure 10. Schema showing the dispersion states of f-MWNTs in PP/EVA blends: (a) aggregated f-MWNTs in dispersed EVA phase in PP/EVA (80/20) at low load; (b) migration of f-MWNTs to PP phase to form a local “single-network structure” at high load; (c) well-dispersed f-MWNTs in continuous phase of EVA in PP/EVA (60/40) at low load and (d) network formation of f-MWNTs in the whole blend ^[133]. High and low loads refer to 2 wt. % and 0.5 wt. % of f-MWNTs in the blends. Copyright 2009. Reproduced with permission from Elsevier Sci. Ltd.

Nayak et al. ^[134] functionalized MWNTs by coating them with TiO₂ to alter the selective distribution of nanotubes within the (70/30) PA66/SAN blend. It was revealed that unmodified MWNTs tended to localize in the PA matrix in the final stage of mixing after they first dispersed inside the SAN during the early stage of mixing. Further, by coating MWNTs with TiO₂, they remained inside the SAN minor phase. It was suggested that possible hydrogen bonding between Ti-OH groups of TiO₂ and CN groups of SAN is the driving force for this migration. A schematic view of the localization of unmodified and TiO₂-modified MWNTs inside PA/SAN is illustrated in **Figure 11**.

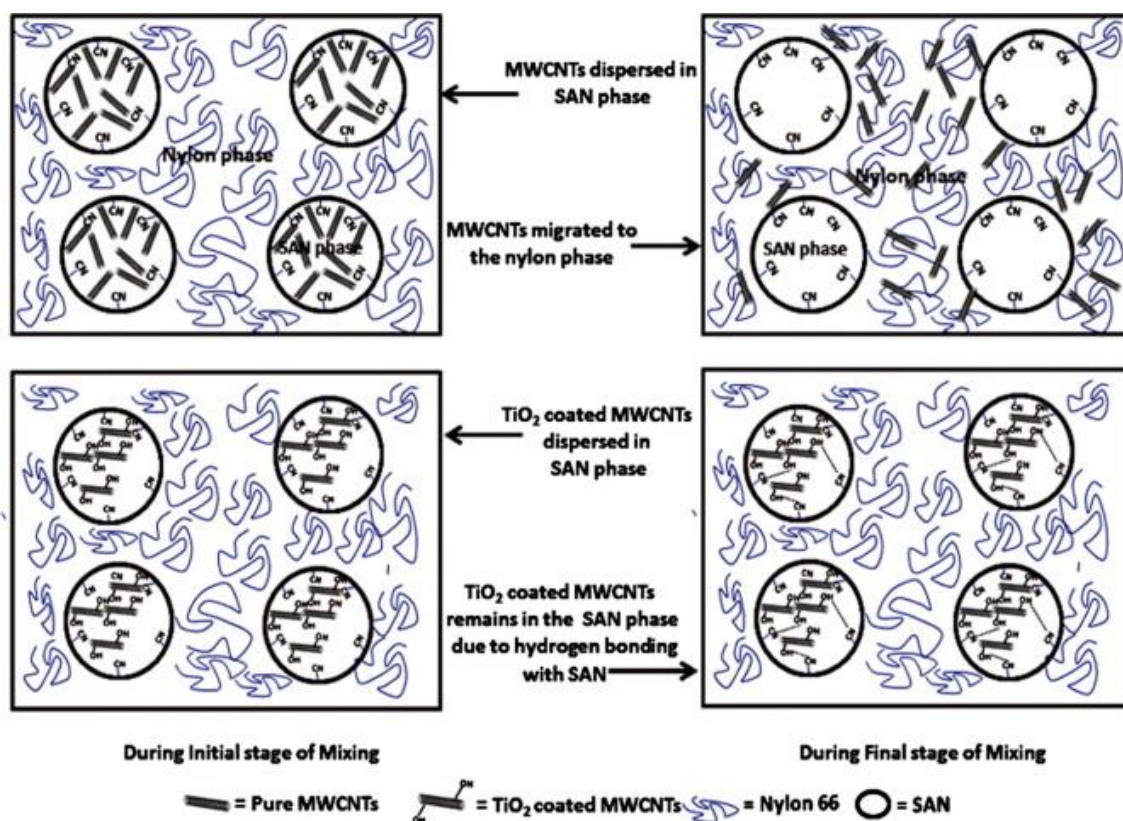


Figure 11. Schematic view of the migration process of unmodified and TiO_2 -coated MWNTs during mixing^[134]. Copyright 2012. Reproduced with permission from Elsevier Sci. Ltd.

Despite successfully changing the selective localization of MWNTs by modifying them, the mechanical properties of the blends with MWNTs inside the PA matrix phase were superior to those with modified MWNTs inside the SAN minor phase due to the interruption of load transfer within the blend, as all nanotubes are restricted inside the lower volume (SAN). This elucidates how different particle localizations in an immiscible blend can influence the final properties. Therefore, it is crucial to design the formulation and processing in a way that nanoparticles can be advantageous to the system. In another study, Tao et al.^[135] investigated the effect of CNT modifications on the migration of nanotubes within EA/PA12 blends. CNTs were grafted or coated with PMMA and PS, as the interfacial confinement of PMMA and PS in EA/PA blends was known previously. Therefore, CNTs were modified (grafted or coated) with PMMA (PS) were premixed with the minor PA12 phase and blended with the EA matrix. The findings revealed that PMMA (PS)-grafted CNTs were able to migrate toward the interface depending on the droplet size such that in smaller domains the chances of reaching the interface was believed to be higher than in larger domains where the distances of nanotubes to the interface were still large. On the other hand, PMMA (PS)-coated CNTs remained inside the PA12 due to the convenient desorption of weakly bonded (non-covalent) polymer chains from the surface of CNTs.

However long chain PS was found to be more effective in inducing migration of CNTs to the interface. Functionalization of MWNTs with PS grafting was practiced in a different blend system: (40/60) SAN/PPE ^[136]. It was found that PS-grafted MWNTs could migrate to the PPE phase, whereas the migration was directly proportional to the molecular weight of the PS.

Bharati et al. ^[137] showed that adding a random copolymer of (PS-r-PMMA) could not affect the state of dispersion of amine-functionalized MWNTs in PαMSAN/PMMA blends, although they influenced the blend morphology by encapsulating the PMMA-dispersed phase. Therefore, knowing that nanoparticles tended to move toward the thermodynamically compatible phase and that dwelling at the interface would be more beneficial with respect to morphology stabilization and final properties, nanoparticles can be surface-modified with copolymers made from the same constituent of the blends or with moieties having similar surface energies with both phases to locate them at the interface. Care must be taken when modifying the nanoparticles in favor of final localization of the nanoparticles inside the blends. Zhao et al. ^[138] functionalized the surface of CNTs first with epoxy group and later grafted with long PMMA molecules. The functionalization method used in this study enabled the localization of CNTs at the interface of (50/50) PLLA/PVDF blends by promoting a bridge between the two polymers through interactions between PMMA molecules with PVDF and the reactions between epoxy groups and carboxyl group of PLLA during blending. The bridging mechanism led to compatibilization of the blend followed by a significant decrease in domain size. This was not the case when CNTs were only modified with OH groups or only PMMA as they were all localized inside the PLLA indicating the importance of modifications on the localization and hence compatibilization of the blends.

Alternatively, the mixing protocol can be selected in such a way that migrations toward the other phase are promoted. Speaking of the surface modification of the nanoparticles using surfactants, the possible degradation of the surfactants must be also considered as the quaternary ammonium group on the surface of the alkylamine modified nanoparticles can promote thermal instabilities by causing Hoffman degradation around 180~200°C where the processing temperature ranges of most polymers are within or above these temperatures ^[139, 140]. It is not clear to what extent the possible degradation of surfactant can impede the migrations during melt blending but if that is the case and surfactants can no longer play a significant role in final localization, then it is the viscosity ratio that can determine the localizations where particles move to the phase which melts faster. To have more stable particles at a higher temperature and ensure surface modifications affect the wetting properties hence encouraging migrations, it can be suggested that particles modified with metal-oxides or copolymers will be more efficient, especially metal-oxides if conductive characteristics are of interests.

5.2. Influence of the Particle Size and Shape

Another important aspect of Eq. (11) is that the proposed energy of detachment is proportional to the square of nanoparticle radius. That is, a smaller nanoparticle requires a smaller energy of detachment; hence, nanoparticles with very small size are less effective in stabilizing morphology due to facile detachments from the interface^[128, 130]. However, the total energy per unit volume of a system to remove all the nanoparticles with volume fraction ϕ from interface shows that larger nanoparticles require less energy to be removed from the interface, as shown in Eq. (13)^[141].

$$G_t = \frac{3\phi\gamma_{ow}(1 \pm \cos \theta_{ow})^2}{4r} \quad (13)$$

The positive sign indicates the removal of nanoparticles to the oil phase and the negative sign denotes removal to the water phase. This is in agreement with the report of Krasovitski and Marmur^[142] in which they mathematically calculated the localization of nanoparticles of different sizes in the equilibrium state. The calculations were made on a liquid-liquid system containing spherical liquid drops (liquid-A) dispersed in a fluid (liquid-B). In addition, the particles were considered as spheroids-shaped ones submerged into the drops of liquid-A. They reported that for nanoparticles to either penetrate the dispersed phase or stay in the fluid, the contact angle dependencies would play a vital role. It was calculated that nanoparticles with higher aspect ratios would penetrate the dispersed phase once the contact angle value was less than 90° and they would remain in the fluid matrix if this requirement was not met. Nanoparticles with smaller aspect ratios would gradually penetrate (depending on the variation of contact angle), indicating a narrowed wetting coefficient interval for longer aspect ratio particles at the interface. Göldel et al.^[51] nicely elaborated the work of nanoparticle penetration through the interface of polymer blends with respect to the shape of the nanoparticles. To compare the rate of migration and final localization of nanoparticles, two different types of nanoparticles (MWNT and CB) were simultaneously premixed with the less favored minor SAN and the prepared nanocomposite was subsequently blended with the PC phase. The results revealed more MWNT particles in the PC phase after 5 min melt blending and more amount of CB at the interface compared to that of MWNTs, knowing that both nanoparticles used were more thermodynamically favored toward the PC phase. The authors proposed a “Slim-Fast Mechanism” (SFM) to explain that particles with higher aspect ratio (rod-like such as MWNT) migrate faster than those with lower aspect ratios (spheroids such as CB). It was proposed that interfacial curvature instability is the driving force for the migration of nanoparticles. When an individual one-dimensional nanotube is perpendicular to the direction of the interface, it has the maximum instability with constant curvature throughout the penetration process; relaxation occurs when migration is done, while in the case of spherical nanoparticles, the

interface relaxes during penetration. Therefore, nanoparticles with high aspect ratios would migrate faster since the curvature cannot relax when the equilibrium wetting angle does not change due to constant instability of the curvature. However, in a more non-ideal (realistic) situation, nanotubes exist in the form of agglomerations or random coiled structures. In such a case, penetration happens in the sequence: (i) the sections of nanotubes that are perpendicular to interface, (ii) the sections where tube length is parallel to the interface, and (iii) coiled section, as shown in **Figure 12**. This could explain why some of the nanotubes were at the interface after 5 min of melt blending. Those found in the PC followed the proposed SFM route to migrate. The speed of transfer for different particles was then tabulated (**Table 3**) based on their shape (aspect ratio).

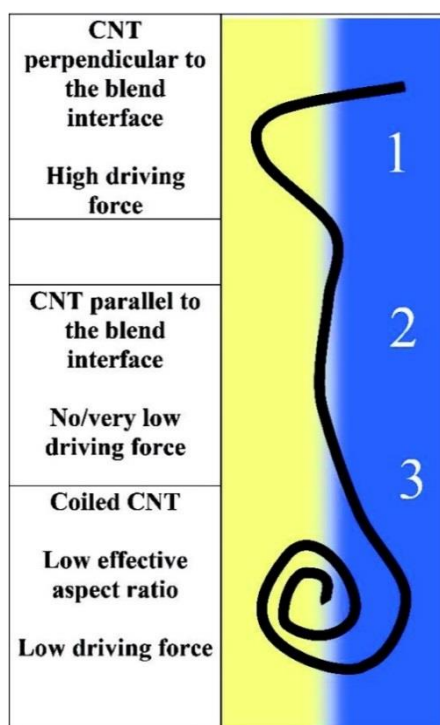










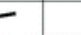


Figure 12. CNT shape-dependent efficiency of the SFM. Transfer takes place in the order (section 1 > section 2 > section 3) ^[51]. Copyright 2011. Reproduced with permission from the American Chemical Society.

Table 3. Transfer rates of different particles with respect to their aspect ratios ^[51]. Copyright 2011. Reproduced with permission from the American Chemical Society.

The Slim Fast Mechanism (SFM)						
Group I: Low aspect ratio objects – slow transfer – high interfacial stability						
Class	CNT	CNT	CB	CB	CB	MMT/Clay/Graphite
Scale	Macro-micro	Micro	Meso-micro	Micro-nano	Nano	Micro
Description	Primary agglomerate	Coiled CNT	Agglomerate	Aggregate	Nano-Aggregate	Stack
Scheme						
Intermediate transfer speeds/interfacial stabilities		Group II: High aspect ratio nano objects – fast transfer – low interfacial stability				
Class	MMT/Graphene/Silica	CNT	CNF	Halloysite	Other Nanotubes and -fibers	
Scale	Nano in 1 dimension	Nano in 2 dimensions	Nano in 2 dimensions	Nano in 2 dimensions	Nano in 2 dimensions	
Description	Exfoliated or single sheet	Separated, linear CNT	Separated, linear CNF	Separated, linear tube	Separated, linear tube	
Scheme						

Recently, Dil and Favis ^[36] found that both micro- (300 nm) and nano-sized (100 nm) silica particles migrated to the interfaces of PLA/PBAT blends when they were premixed with the less favorable PLA, regardless of their sizes. It is stated that the time that it takes to drain the film before particles meet the interface is proportional to particle size and the viscosity of the particle-embedded phase. Therefore, nano-silica particles were found to be more effective in draining the PLA film and wetting the interface than larger micro-silica particles. It should be noted that the migration is also a function of the viscosity of the PLA used in this study, which will be discussed in section 5.3.

In summary, it can be concluded that the major part of this section is devoted to the penetration stage of the nanoparticles at the interface area. Nanoparticles with larger aspect ratios penetrate to the other component faster due to instabilities at the interface. On the other hand, nanoparticles with lower aspect ratios take longer to penetrate. If one intends to immobilize particles at the interface based on the desired properties, care must be taken during processing not to exceed the migration to the other phase if long aspect ratio nanoparticles are being used. We appreciated the very useful findings of the above mentioned articles, yet there are some concerns that need to be investigated. It will be more useful if the nanoparticles used are of exactly the same type when comparing the migration rates. For example, if the effect of aspect ratio were concerned, different nanotubes of the same diameter and surface modification would be more interesting to understand the issue more clearly. However, it should be noted that long aspect ratio nanoparticles could exist in agglomerates with more curves, and therefore, there is a higher possibility of shortening of length during processing, which can affect the quality of dispersion ^[143]. The other parameter is the surface modification, if the different nanoparticles being studied are modified it is not clear

whether the higher concentration of surface functionalities on the nanoparticles with higher surface areas can play a boosting effect and if yes, to what extent. A higher surface area can also increase the possibilities of agglomerations. In practice, nanoparticles tend to agglomerate or entangle in the case of nanotubes, thus, migrations may occur in clusters or individuals or even first disentangle and then migrate. Moreover, nanotubes are susceptible to breakdown (chopped) into smaller sizes during melt blending, meaning the higher the aspect ratio the higher the possibility of breaking ^[144]. Therefore, it will be interesting to know what extent of the migration could be due to the particles breakdown. Considering all the possibilities, the migration mechanism seems to be a more complex process and more investigations at least in terms of particle size and shape can be done.

5.3. *Influence of the Viscosity Ratio*

As discussed earlier (Section 3), migration of nanoparticles inside the molten polymers are translational (convection mode) and such phenomenon may not occur under static conditions. Considering the requisite thermodynamic and other kinetic conditions (e.g., force, mixing time, etc.) exist to stimulate the migrations, at a given time migration rate is a function of viscosity. The higher the viscosity the slower migration rate will be.

Maiti et al. ^[145] stated that when the viscosity of (epoxidized natural rubber) ENR increased in (natural rubber/ENR) (NR/ENR) blends, more silica nanoparticles were found in the NR phase despite better affinity with the ENR phase, as the higher viscosity of ENR retarded migration from NR to ENR. Note that silica nanoparticles were incorporated in equal proportions into single rubbers (ENR-silica and NR-silica) before blending them together. Gubbels et al. ^[69] reported that the total migration time was longer when CB nanoparticles were premixed with a higher viscosity PE phase. That is, penetration of CB particles through the phase with higher viscosity PE to the other one with lower viscosity PS was a more time-consuming process. Zaikin et al. ^[146] also reported that increasing the viscosity of the PMMA or PE retarded the migration of CB from PE to PMMA and from PS to PE, respectively. Moreover, they found that CB particle localization at the interface was more likely when CB was premixed with the less favorable phase and then blended with the more thermodynamically favored phase. In their study considering the more affinity of the CBs to be localized at the interface, CBs were premixed with each polymer before blending with other virgin polymer. Dil and Favis ^[36] found that when higher viscosity PLA was used larger silica particles (micro-silica) remained inside the PLA phase while nano-silica particles could migrate to the interface. When silica particles were premixed with low viscous PLA they migrated toward the interface during the blending with PBAT due to thermodynamic driving forces, while the majority of the silica particles remained inside the PLA phase when higher viscosity PLA was

used, indicating that viscosity can play a substantial role in the migration of particles. Plattier et al. [147] extensively studied the effect of viscosity ratio on the localization of CBs in co-continuous (60/40) PP/PCL blends. A series of blends with different viscosity ratios (0.06, 0.3, 1.1, 3.5, and 14.7) were prepared and CBs were added when the polymers were already molten to avoid the effects of first molten phase localizations. Table 4 summarizes the different blends with their corresponding viscosity ratio used in this study.

Table 4. Viscosity ratios of the blends used in this study [147].

Blend	Viscosity Ratio η_{PCL}/η_{PP}
PP4/PCL1	0.06
PP4/PCL2	0.3
PP2/PCL2	1.1
PP3/PCL3	3.5
PP1/PCL3	14.7

It was revealed that CBs were located in the higher viscosity phase. CBs were found in PP at the lowest viscosity ratio (0.06), in PCL at the highest viscosity ratio (14.7), and at the interface when viscosity ratio was nearly 1 (1.1). Although predictions based on wettability coefficients offered a better affinity for CBs toward the PCL, the results showed that viscosity ratio could significantly interfere with the final localization. The authors proposed a model (Eq. 14) that describes the influence of each component's drag force on the ejection of trapped particles (illustrated in **Figure 13**) at the interface.

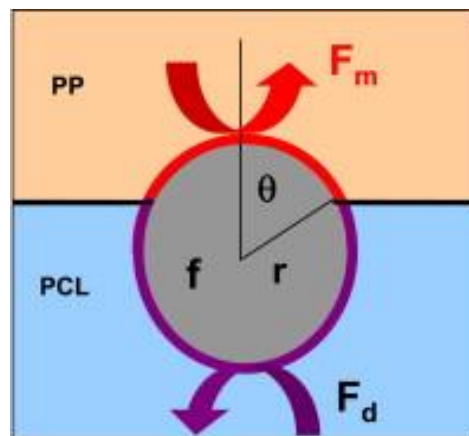


Figure 13. Schematic illustration of a particle at the interface between PP and PCL [147]. Copyright 2015. Reproduced with permission from Elsevier Sci. Ltd.

$$\frac{F_d}{F_m} = \frac{(1 + \cos \theta)}{(1 - \cos \theta)} K \quad (14)$$

where θ is the contact angle at the interface, K is the viscosity ratio and F_d and F_m represent drag forces from PCL and PP, respectively. This implies that drag forces are proportional to the contact angle and viscosity ratio, suggesting that when viscosity ratios were near 1, drag forces were similar and hence, particles remained at the interface. On the other hand, once the viscosity of one of the components increased, the particles were dragged into the more viscous one. Note that the results and model account for the situation where particles are already at the interface and do not discuss the situation when particles are initially embedded in one of the phases. Similar behavior was reported by other researchers as well [148, 149]. Persson and Bertilsson [148] found aluminum borate whiskers in the phase with higher viscosity in most blend cases observed in their study. One cannot make a firm conclusion on the localization of the whiskers solely based on the viscosity ratios as thermodynamic effects can also play an important role. Xiong et al. [149] showed that in an ABS/PC/MWNT system, nanotubes would migrate to the ABS phase from the PC/MWNT masterbatch at a shorter mixing time when high viscosity ABS with higher rubber content was used, despite the higher affinity of the nanotubes toward the PC phase. However, at a longer time the nanotubes migrated back to the PC phase. They argued that the migration mechanism lies in morphology changes during mixing, where, during early stages of mixing the rubber part, which has more affinity toward the MWNTs are more exposed to the surface and MWNTs due to the formation of PC ribbons and cylinders; therefore, they can interact with nanotubes. In the late mixing stage, the broken-up PC dispersed phase favored lower chances for the rubber part and MWNTs to meet due to the change in the structure of the rubber molecules. Therefore, MWNTs migrated back to the more favored PC phase. Although a reasonable mechanism as a result of morphology changes was proposed, the main reason for these changes (droplet break up), which is the change in the viscosity ratio and consequently capillary number, was never mentioned, as discussed in section (4.3). These results are in contrast with the model (Eq. 11) proposed by Levine et al. [128] as interfacial energies, contact angles, and particle size were the main parameters determining the required energies to drag particles; viscosity ratio was not considered. Feng et al. [150] found that CB particles would locate in the lower viscous phase in a PP/PMMA blend. As the viscosity of PMMA increased, CB particles moved toward the interface and eventually to the phase with the lower viscosity (PP) despite predictions based on wettability coefficient parameters that estimated the accumulation of CBs in the PMMA phase. Le et al. [151] reported that changing the molecular weight of NR in NR/SBR blends did not have a significant effect on the final localization of CB in the blend. It was revealed that CB particles were first wetted by the NR phase regardless of the molecular weight; they then migrated toward the SBR phase due to better rubber-filler interactions.

Eventually, it is obvious that viscosity can have a role in the rate of migration. However, the thermodynamic effect determines the final localization and viscosity can only hinder or accelerate the adsorption/desorption rate of the polymer on the particles. Therefore, it is difficult to consider viscosity as an independent conclusive factor determining the localization of nanoparticles where thermodynamic and other kinetic factors are more crucial. To be more specific, viscosity ratio may have a stronger influence on the migration of nanoparticles than their distribution in a single-step melt blending situation. As mentioned previously nanoparticles migrate to the more thermodynamically favored component under sufficient supplied force and mixing time. Therefore, the viscosity in which nanoparticles are preliminarily embedded determines the migration rate. This effect would be more tangible if sequential blending is being practiced. Moreover, as discussed previously viscosity ratio plays an important role in droplet deformations so in cases where viscosity ratio promotes the droplet breakup, higher collision chances with the nanoparticles sitting in the thermodynamically unfavored component can be expected.

Furthermore, since viscosity and mixing time are important here, it must be noted that some polymers undergo thermal and oxidative degradation during mixing when exposed to high temperatures and oxygen. This leads to a significant change in their molecular weights and in turn viscosities. For example, PLA^[152] is a type of polymer which thermally degrades and its viscosity could decrease due to thermal degradation during processing if it is sheared above a certain time, or on the other hand, polymers like PA6, PET, and PE can undergo thermo-oxidation which leads to branching and cross-linking reactions^[117-119, 153, 154] which in turn increases their viscosity over time. Therefore, when designing a blend, a suitable blending protocol should be considered to avoid such influences especially when particle migrations are needed. Using proper anti-oxidants, ambient (nitrogen) and extrusion methods could be a solution when mixing time is shorter and shearing forces are higher compared to internal mixers.

6. Migration Induced Electrical Conductivity

6.1. Introduction

This section attempts to address the electrical conductivity of the immiscible polymer blend composites with respect to the dispersion of the conductive nanoparticles and processing conditions. More specifically, the discussions are centered on the role of nanoparticles migration in immiscible polymer blends and how the process of migration can induce the electrical conductivity of final composites. Formation of a filler network^[155] and/or hopping/tunneling^[156, 157] are the main conduction mechanisms in filled systems, both depending on the filler concentration to ensure the minimum required inter-particle distances for a conductive network. The corresponding

minimum filler concentration where electrical conductivity dramatically increases is defined as the electrical percolation threshold (Φ_c). Equation (15) shows the relationship between conductivity of the filled polymers with the filler concentration.

$$\sigma = p(\varphi - \varphi_c)^t \quad (15)$$

where σ is the conductivity of the filled polymer, φ is the filler concentration, p represents the intrinsic conductivity of the filler, φ_c is the concentration corresponding to the percolation threshold, and t is the critical exponent associated with the dimensionality of the composite system [69, 158, 159]. Model calculations predicted values of t in the range 1.1–1.3 correspond to a two-dimensional system while values between 1.6 and 2.0 correspond to a three-dimensional system [160].

There have been many attempts to model the percolated systems and predict the percolation threshold concentrations or resistivity of a system. McGee [161] developed the Equation (16) for prediction of critical concentration of the anisotropic cylindrical shaped particles. The corresponding model was presented as shown in (Eq. 16)

$$v_c = N_c(\pi d^2 L)/4V \quad (16)$$

where v_c is the critical concentration for the formation of percolation network, N_c is the total number of cylinders at the critical concentration, d and L are the cylinder diameter and length, respectively and V the total volume. Fournier et al. [162] proposed a model (Eq. 17) defining the insulating-conductive transition.

$$\log \rho = \log \rho_f + \frac{\log \rho_m - \log \rho_f}{1 + \exp[b(p - p_c)]} \quad (17)$$

Here, ρ_m and ρ_f are the matrix and composite resistivity, respectively. The change of conductivity at the percolation threshold p_c is dictated by the empirical parameter b . This current proposed model and its modified versions have been extensively used to describe the conductive structure of the composites [163-165]. In many other studies, computational simulations were used to describe the percolation thresholds in polymer composites majorly with the help of the Monte Carlo technique [166-173]. Despite all the efforts to predict and describe the percolation thresholds and insulator-conductive transitions in polymer composites, limited work on the modeling and simulation of such phenomenon have been done on polymer blends since morphology becomes more complicated. Taipalus et al. [174] used the fiber-contact model (FCM) to predict the electrical conductivity of the PP/PANI blends filled with carbon fibers. In this model, the effect of fiber to fiber contact and fiber length on the conductivity of the composites are included. In their work, they modified the current model by taking the conductivity of the polymer matrix into account. Recently, Bai et al. [37] developed a model describing the relationship between interfacial rheology,

electrical conductivity and morphology of the co-continuous blend of PLA/PS loaded with r-GO. In their study, they assumed only graphenes at the interface were involved in the conductivities. Moreover, the thickness of graphene oxide sheet layers at the interface and characteristic domain size was taken into account here. It was shown that both interfacial modulus and electrical conductivity exhibit a power law behavior with respect to characteristic domain size increments. All the aforementioned studies indicate the role of conductive network formation. It is always recommended to have a lower percolation threshold to avoid extra production costs and flexibility of materials related to the high filler contents ^[175]. However achieving the compromised desired properties at low filler concentrations has been a challenge. Phase separation in immiscible blends allows us to tune microstructures by adjusting the thermodynamic and kinetics parameters, e.g., blending sequence, time, viscosity ratios, type of the particles, etc., each of which has been discussed earlier. This in turn can affect the migration as well as localization, and hence the final electrical conductivity. One of the ways to obtain such an outstanding combination of properties is to fabricate co-continuous polymer blends incorporated with conductive fillers to have “double-percolation” behavior ^[30, 176]. The benefit of having a double-percolated structure is that a less conductive filler is needed to form a percolated conductive network. In addition, it is worth mentioning that the percolation threshold decreases with increasing aspect ratio of the filler ^[158]. Previously, we have also discussed in section (5.3) that particles with longer aspect ratios migrate faster according to the “Slim-Fast Mechanism” ^[51]. Therefore, in this section we address how the migration of conductive particles with different shapes and aspect ratios (L/D) can influence the conductivities of the final blends.

6.2. Carbon Black

Tchoudakov et al. ^[64] studied the effect of the mixing sequence on the resistivities of PP/PA blends incorporated with CB at different blend compositions. The compositions covered in this study are shown in **Table 5** with respect to different mixing sequences.

Table 5. The blend composition studied in reference ^[64] with respect to the different mixing sequences. The numbers in brackets indicate the weight percentage of the components in order of (PP/PA).

Sequence 1: CB was added to the molten blend		
Sequence 2: CB was premixed with PP followed by addition of PA		
Sequence 3: CB was premixed with PA followed by addition of PP		
Sequence 1	Sequence 2	Sequence 3
(100/0)	(100/0)	(100/0)
(90/10)	(90/10)	-
(80/20)	(80/20)	-
(70/30)	(70/30)	(70/30)
(50/50)	(50/50)	(50/50)
(40/60)	-	-
(30/70)	(30/70)	(30/70)
(10/90)	-	-
(0/100)	(0/100)	(0/100)

It was shown that despite the better affinity of CB to PA, the blends with premixed PP and CB to which PA was added later ((PP/CB) + PA) had the lowest resistivity of nearly 10^4 om-cm at (70/30) PP/PA blend with 8 phr CB compared to sequence when CBs were premixed with PA at the same composition. This indicates that the thermodynamically driven migration of CBs from PP to PA can promote conductivity in the blends (migration-induced conductivity). The high resistivity of the blends of premixed PA with CB followed by the addition of PP ((PA/CB) + PP) at PP-rich concentrations was suggested to be due to the spherical morphology of the blends with PA/CB droplets isolated from the neighboring droplets failing to form interconnections between CBs. Later on, the same group ^[177] used the same procedure ((PP/CB) + PA) wherein PA was the dispersed phase to study the potential of the current blends as sensor materials. Blend composition was chosen in a way that a double-percolation system was achieved for better conductivity behaviors where CB particles were found to be at the interface between the phases due to thermodynamically driven migration, similar to the work of Soares et al. ^[178] where the lowest resistivity was attained when CB was at the interface of the co-continuous PS/PIP blend. Srivastava et al. ^[177] investigated the resistivity of the (75/25) and (70/30) PP/PA6 blends filled with CB which claimed to have double-percolation structure at different shear rates. It was revealed that resistivity fluctuates with shear rate for (70/30) blends having slightly lower resistivity than the (75/25) blends at all shear rates. This indicates the sensitivity of the double-percolation systems to perturbations such as shear rate. A significant production shear-rate dependency of resistivity was found for the blends exposed to different chemical components. It was also shown that the resistivity of the blend gradually increased during exposure to chemicals and it dropped when samples were dried in air after cutting the exposure. This cycle was shown to

be repeatable, indicating the potential of the blend for sensing applications. During exposure, polymer phases swell and CB particles at the interface may facilitate the penetration of liquids leading to destruction of the networks. On the other hand, when exposure stops and the sample is being dried, a deswelling mechanism proceeds resulting in decreasing the resistivity and limited rearrangement of the networks. Therefore, selection of a blend and particle localization for a particular sensor application is important, depending on which phase is sensitive to the exposed chemicals and to what extent they can tolerate swelling/deswelling cycles.

Gubbels et al. ^[66, 69] found that the lowest percolation threshold was achieved when CB was found at the interface of the co-continuous (45/55) PE/PS blend. The resistivity increased again at higher mixing times due completion of the migration toward the PE phase (**Figure 14**).

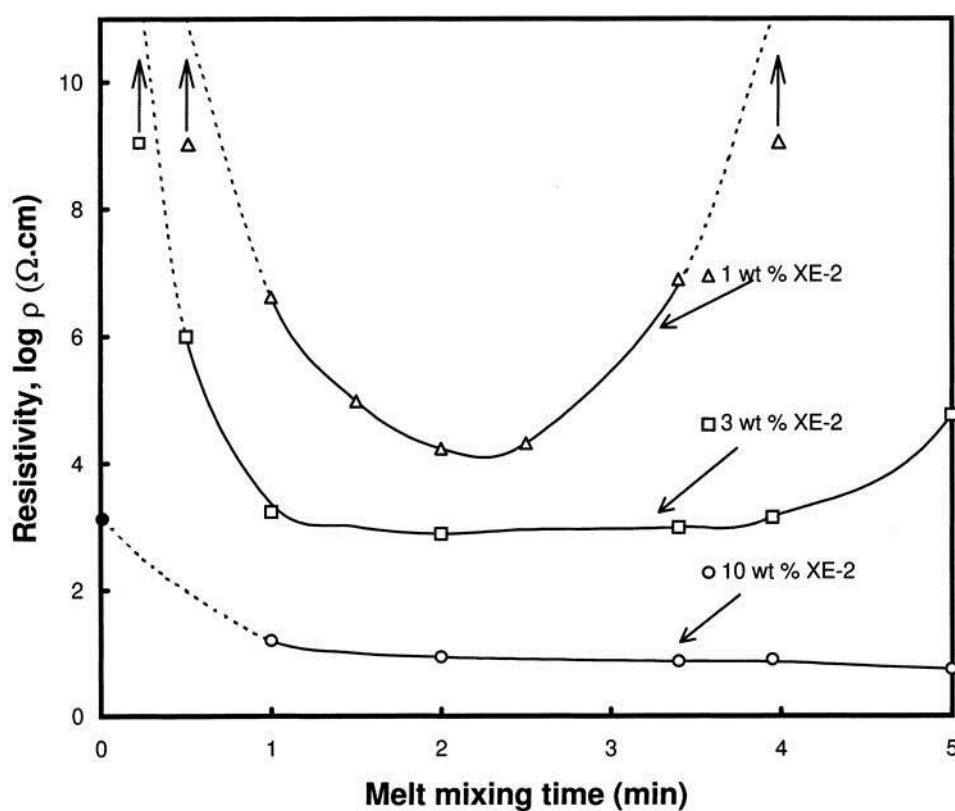


Figure 14. Influence of mixing time on the resistivity of 45/55 PE/PS blends filled with different XE-2 concentrations. XE-2 carbon black was premixed with PS before blending ^[69]. Copyright 1998. Reproduced with permission from the American Chemical Society.

Alternatively, Zaikin et al. ^[146] stated that the lowest electrical resistivity was attained when CBs were located at the interface of immiscible (1:1) PP/PS blends. As it is known that CB particles are more thermodynamically favored at the interface, they were premixed with each polymer PP (PP+CB) or PS (PS+CB) before blended with the second unfilled polymer to monitor the effect of CB migration towards the interface on the electrical resistivity. The electrical

resistivity reduced when blends were mixed for a longer time and reached a constant minimum value indicating the equilibrium state was reached when the CB particles migrated to the interface.

Li et al. [67] studied the effect of the mixing procedure on the morphologies and conductivities of (70/30) PE/PET blends filled with 7.5 and 15 phr CB. The idea was to make electrically conductive *in situ* microfibrils by compounding previously mixed PET/CB composites with PE. Later the quenched extrudates went through post-processing conditions at temperatures identical to the processing temperature of PE to produce solidified networks of PET/CB *in situ* microfibrils. It was found that CB located in the PET phase formed an interconnected network of *in situ* microfibrils, resulting in a lower percolation threshold than the simultaneously mixed blends of PE/PET/CB. In a further study, the same group [68] compared the influence of CB type and concentration on the morphology and electrical conductivity of PE/PET/CB blends with the results of the previous study using the same production protocol as for PET/CB microfibrils where the volume ratio of PET and PE was 1/3.2. Two different types of CBs used in these studied showed different percolation thresholds, although both were located inside the PET phase (**Figure 15**).

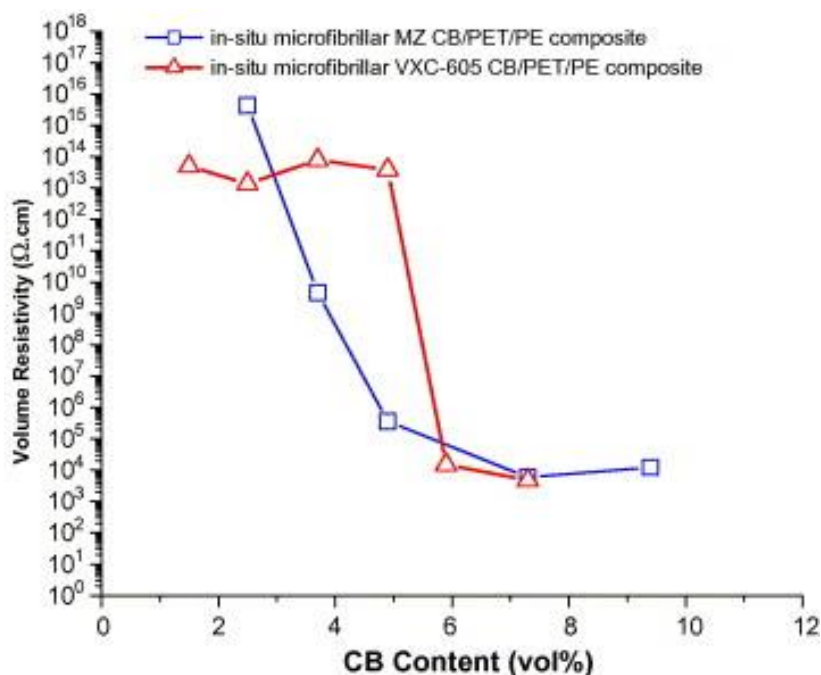


Figure 15. Volume resistivity of PET/PE blends incorporated with different carbon black fillers (MZ CB and VXC-605) [68]. Copyright 2005. Reproduced with permission from Elsevier Sci. Ltd.

The difference was explained to be due to the maximum packing concentration of the nanoparticles. As the concentration increased, some nanoparticles migrated to the surfaces of the PET/CB microfibrils due to the saturated available volume. It was discussed that while CB particles were solely in the PET phase electrons could not transport between the microfibrils, while at higher concentrations those CB particles at the surface of PET/CB microfibrils facilitated

electron pathways through the network of neighboring microfibrils. In other words, this particular polymer blend system was electrically insulating up to a critical concentration where CB particles were completely inside the PET phase; above this concentration where some CB particles were found at the surfaces of PET it became conductive. That is, nanoparticle localization at the interface is an important factor to obtain a low percolation threshold. Further, it was found that thermal treatment of the PE/PET/CB composite with CB concentrations above the percolation threshold in an inert atmosphere can improve the conductivity of PET/CB microfibrils ^[70]. In such a technique, composites went through isothermal treatment at different times at 180 °C (above the melting temperature of PE matrix), as can be observed in **Figure 16** after each isothermal treatment the same materials went through a temperature ramp up to 180°C. The resistivity-temperature dependence of the composite was measured. If the electrical resistance increases when the temperature rises, the material has a positive temperature coefficient of resistivity (PTCR) (beyond 130°C in **Figure 16**). It was found that the PTCR of the composites decreased with thermal treatment for longer times. In other words, the resistivity of the blends that were treated longer at the isothermal temperature of 180°C (600 min) decreased compared with the case where they were treated for shorter time (3 min).

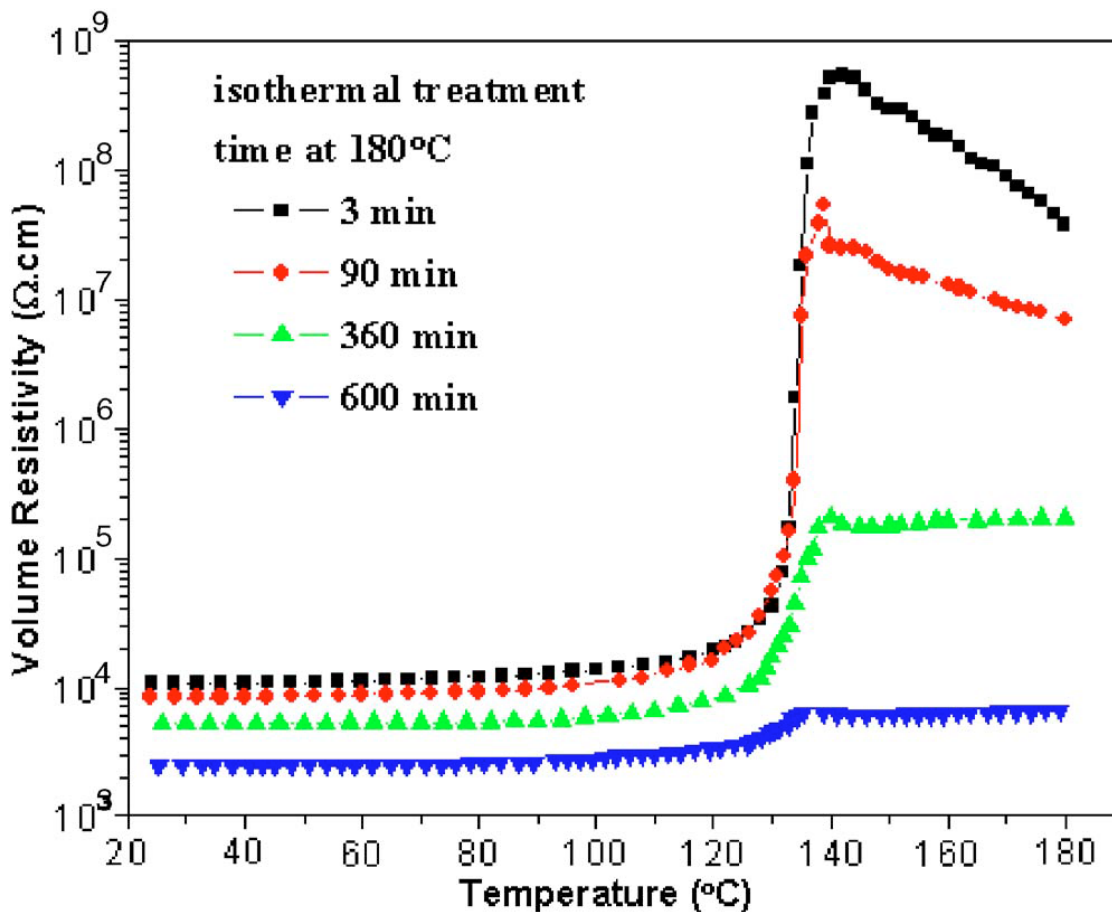


Figure 16. Temperature-dependent volume resistivity of *in situ* microfibrillar PE/PET/CB nanocomposites after isothermal treatment at 180 °C for different lengths of time ^[70]. Copyright 2006. Reproduced with permission from the American Institute of Physics.

It was proposed that more CB aggregates build up on the surface of PET/CB microfibrils at higher temperatures, which retained their shape upon cooling as well. This resulted in more stable and more conductive pathways with thermal treatment time. This could be due to the migration of more CB particles because of the drastic change in viscosity ratio between the neighboring molten PE matrix and PET/CB microfibrils. **Figure 17** shows a schematic illustration of CB rearrangements upon thermal treatment.

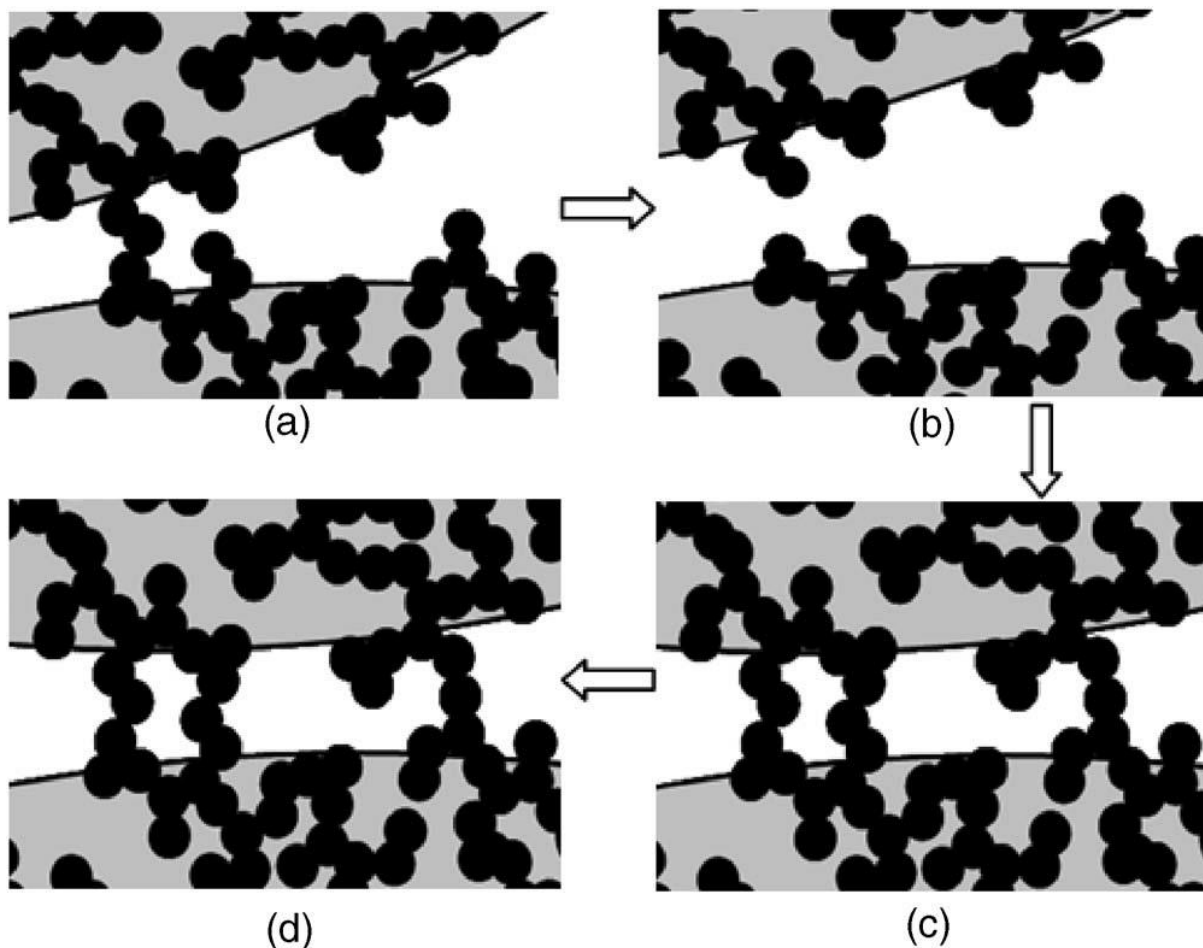


Figure 17. Schematic view of the conductive microfibrillar network formations during thermal treatment. It represents the arrangement of CB fillers on the surface of PE/PET microfibrils at (a) room temperature, (b) after PTCR (beyond 130°C where a sudden increase in resistivity was observed), (c) after isothermal treatment at high temperature, and (d) after cooling down to room temperature ^[70]. Copyright 2006. Reproduced with permission from the American Institute of Physics.

Continuing the previous research, Dai et al. ^[71] produced microfibrils using the opposite approach (note that the volume ratio of the PET/PE was the same as the previous study as 1/3.2). CB was first premixed with PP and further blended with PET as the dispersed phase. The extrudates were then quenched immediately after the slit die. It was shown that CB particles migrated from the PE phase toward the surface of PET during the melt mixing process and later the crystallization process during the quenching phase did not alter the position of CB particles at the interface. This result suggests that when CB particles covered the surfaces of the PET microfibrils (as shown in **Figure 18**), the percolation threshold decreased from 6.8 ^[71] for simultaneously mixed blends (PE/PET/CB), to 5 ^[68] for (PET/CB)/PE, and eventually to 3.8 vol% ^[71] for (PE/CB)/PET with higher conductivities at high CB concentrations for the latter case (plotted in **Figure 19**). This indicates that production protocol could play a significant role in the final localization of particles and hence the conductivity.

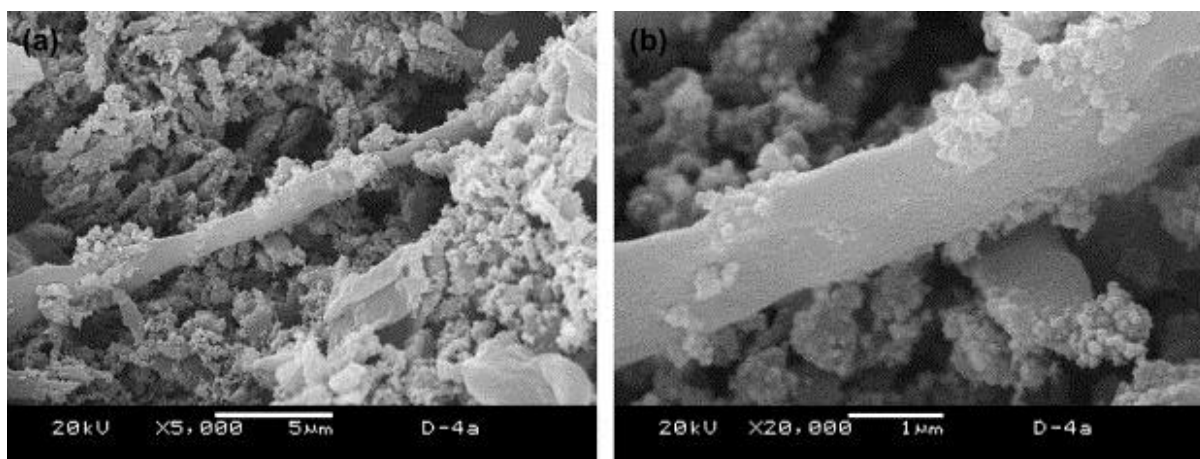


Figure 18. (a) Low- and (b) high-magnification SEM images of hot stretched nanocomposites (i-CB/PET/PE) with 8.1 vol% of CB. A PE/CB masterbatch was used to make the CB/PET/PE blends ^[71]. Copyright 2007. Reproduced with permission from Elsevier Sci. Ltd.

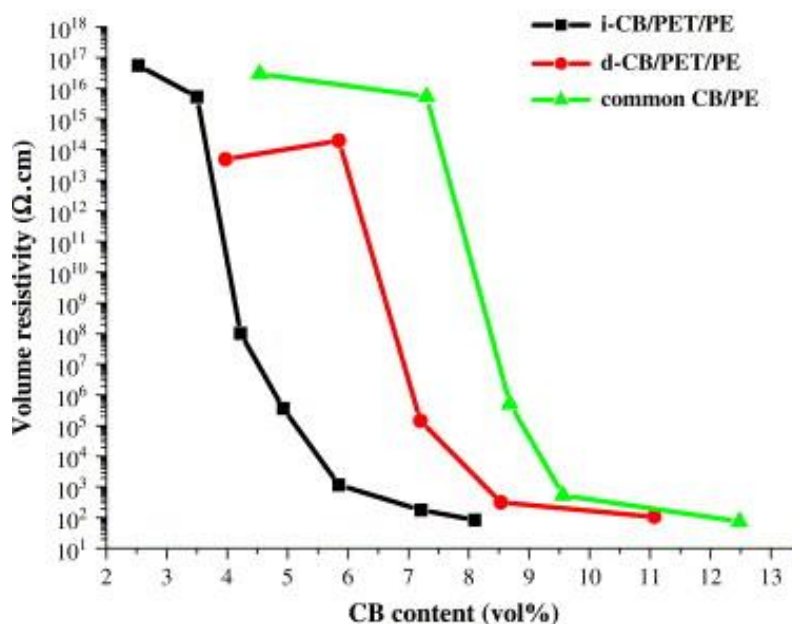


Figure 19. Volume resistivity of the PE/PET/CB nanocomposites as a function of CB concentration for blends prepared with different protocols. i-CB/PET/PE represents the hot stretched nanocomposites where a PE/CB masterbatch was used to make the blends and d-CB/PET/PE represents the directly mixed (simultaneously mixed) blends ^[71]. Copyright 2007. Reproduced with permission from Elsevier Sci. Ltd.

Dharaiya et al. ^[125] found a relationship between the morphology evolution of (90/10) PA6/PP blend filled with 1 wt. % of CB during chaotic mixing and the conductive properties of the blend. At lower mixing times, the conductivity was higher due to the formation of fibril networks. This was followed by a sudden decrease to a minimum conductivity where fibrils were broken up into droplets of PP phase hosting CBs. Eventually, at longer times (high strains) the conductivity increased again due to the migration of CBs from PP to the interface, where dispersed

phase droplets were interconnected through the interfaces. Scherzer et al. [65] showed that conductivities of co-continuous PS/PMMA/CB blends remained nearly unchanged with different mixing sequences. It can be concluded that the volume resistivity in CB-incorporated blends are proportional to the final localization of the CB. It is interesting to note that the optimized volume resistivity was obtained when CB particles were accommodated at interfaces. In the cases where migration of nanoparticles during the processing determines the final localization in the more favored component or interface, the magnitude of migration can affect the resistivity as well.

6.3. CNTs

From the point of view of processing strategy, Gödel et al. [88] investigated the effect of blending sequence on the electro conductivity of PC/SAN/MWNTs blends. It was found that when nanotubes were added to (60/40) PC/SAN blends; the resistivity was lower than the composites of PC or SAN, indicating the higher efficiency of the double-percolated morphologies. Further, it was shown that nanotubes were localized in the PC phase irrespective of blending sequence. Alternatively, conductivity of the blends incorporated with MWNTs remained nearly constant regardless of the mixing sequence (**Figure 20**). Identical results for this particular blend were reported in another study [179]. Interestingly, it has been shown that the addition of *N*-phenylmaleimide styrene maleic anhydride as a reactive component (RC) miscible with the SAN phase can disrupt the conductivity by changing the MWNT localization with nanotubes inside the SAN phase, irrespective of the blending sequence. **Figure 21** shows the electrical resistivity of this particular blend with the reactive component showing contrast with the blends without RC.

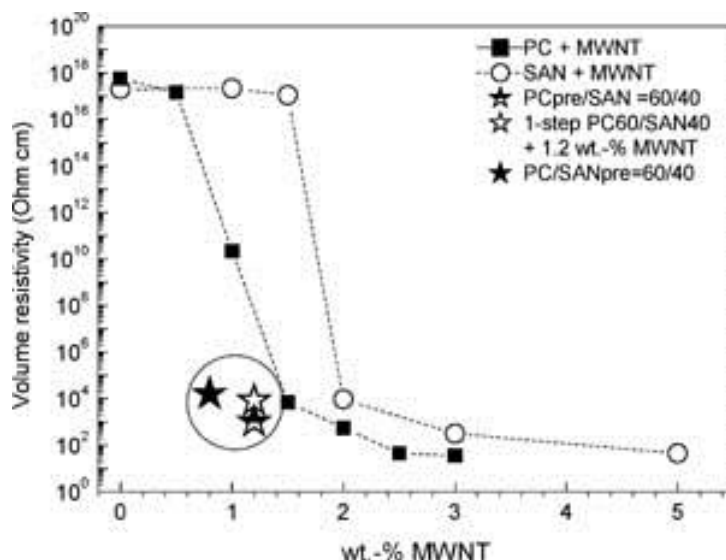


Figure 20. Volume resistivity of PC/SAN/MWNT nanocomposites prepared via different orders of MWNT incorporation compared with single composites. “Pre” indicates the pre-mixture of MWNT with the corresponding phase [88]. Copyright 2009. Reproduced with permission from Wiley-VCH Verlag.

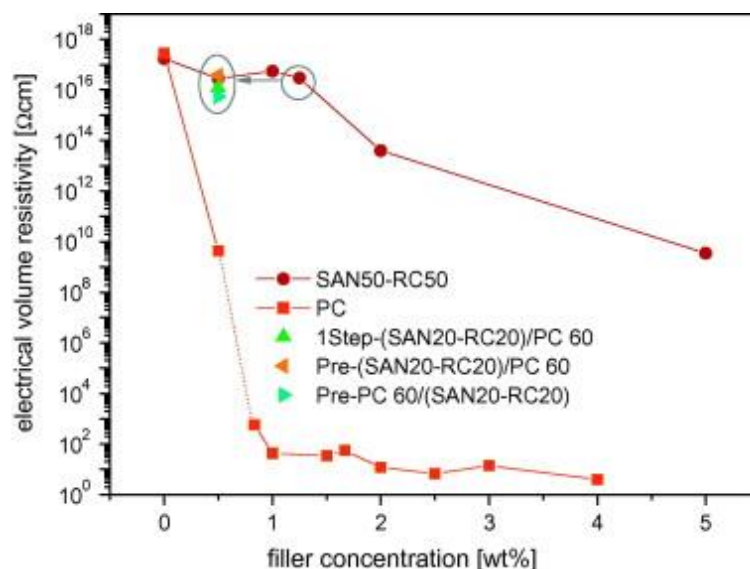


Figure 21. Volume resistivity of PC/SAN/MWNT nanocomposites with reactive component (RC), prepared via different blending sequences. MWNT concentration was fixed at 0.5 wt% for the filled blends ^[179]. Copyright 2011. Reproduced with permission from Elsevier Sci. Ltd.

Li and Shimizu ^[126] studied migration-induced conductivity in PA6/PVDF/CNT blends where higher shear-processing conditions induced the migration of PA6 inclusions hosting CNTs to the PVDF phase (**Figure 22**). Therefore, the conductivities of high shear-processed samples were 5 decades higher than those of low shear-processed ones at 0.6 wt. % of CNT. The cartoon in **Figure 22** depicts a schematic morphology of the nanocomposites and the migration of PA6-laden CNTs into the PVDF upon intensifying the shearing conditions, and their corresponding conductivities.

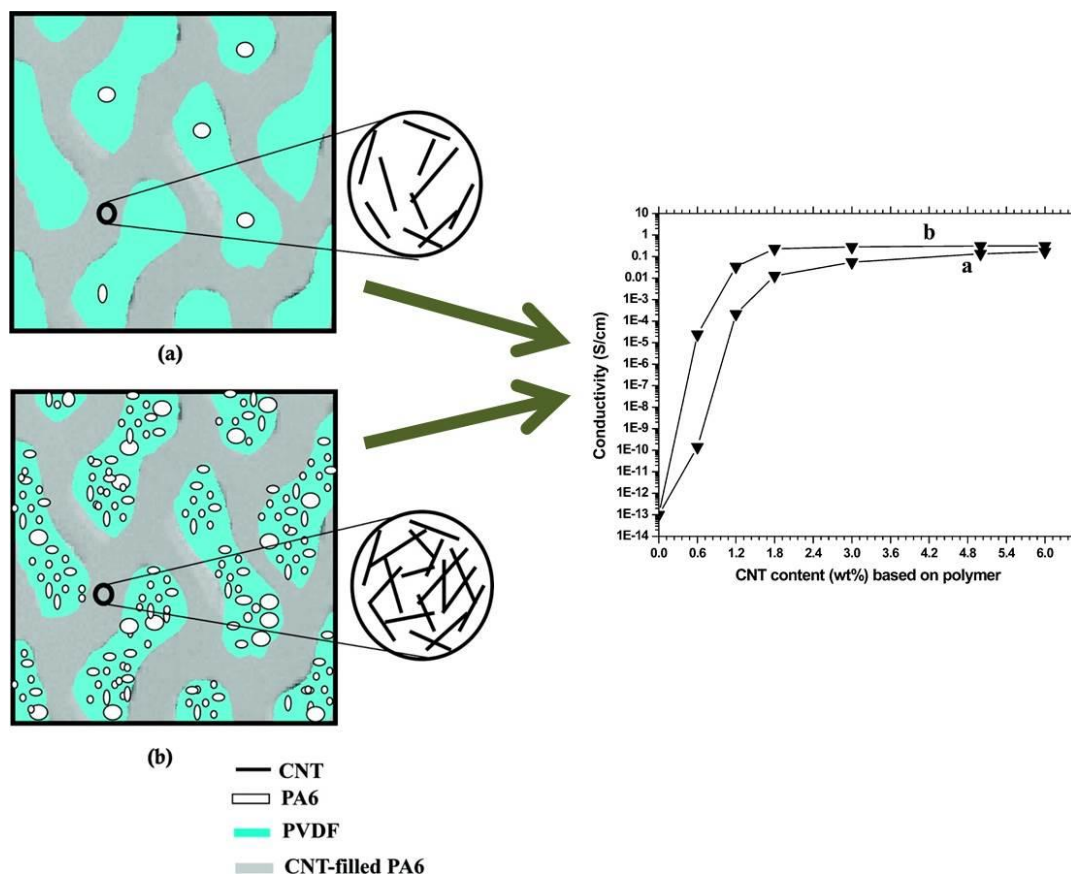


Figure 22. Schematic morphologies of the (a) low- and (b) high-shear processed PVDF/PA6/CNT nanocomposites and their corresponding conductivities ^[126]. Copyright 2008. Reproduced with permission from the American Chemical Society.

Zonder et al. ^[26] investigated the differences in CNT incorporation strategy in PA/PE blends and revealed that the lowest electrical resistivity ($10^8 \Omega \text{ cm}$) and finer morphologies were attained when 0.75 wt.% of CNTs were pre-dispersed in the PE phase in PA-rich blends (75/25) (see **Figure 23**). This was found to be due to the migration of CNTs from PE to the interface during blending owing to better affinity toward the PA phase, which led to the formation of percolating networks, indicating the influence of sequential blending on the final localization and therefore the electrical properties.

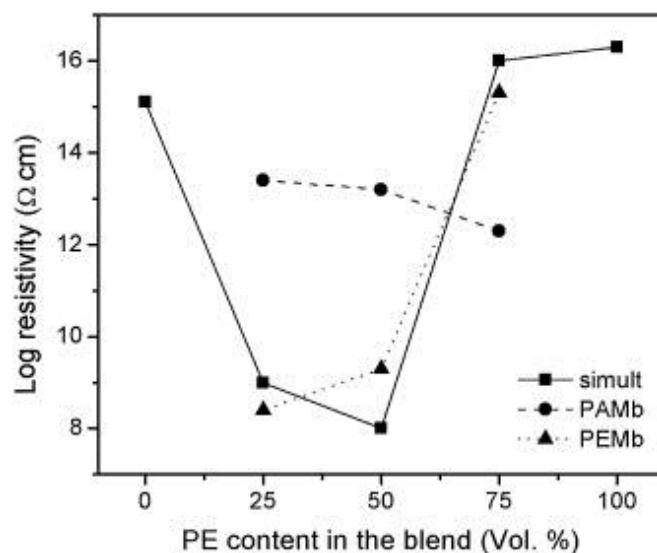


Figure 23. Volume resistivities of PA/PE blends incorporated with 0.75 wt% CNTs simultaneously (simult), pre-dispersed in PA (PAMb), and pre-dispersed in PE (PEMb) as a function of PE concentration^[26]. Copyright 2011. Reproduced with permission from Elsevier Sci. Ltd.

On the other hand, in PE-rich (25/75) PA/PE blend, nanotubes could not make their way toward the PA phase to localize effectively at the interface when they were premixed with the PE phase; therefore, they had higher electrical resistivity (10^{15} Ω cm). This could be due to the higher viscosity of the PE phase when compared to PA, which retards the recoiling process of nanotube aggregates and eventually their migration through the bulk volume of the PE phase to the interface. In blends with PE as the dispersed phase, the distance that nanotubes needed to travel to reach the interface is shorter. Shi et al.^[91] found that CNTs can be immobilized at the interface of (60/40) PLLA/EVA blend during migration from a PLLA/CNT masterbatch phase to EVA after melt blending (refer to **Figure 5**, section 4.1.2). By premixing the particles in a disfavored phase (PLLA), a more conductive final blend with lower percolation threshold could be obtained (**Figure 24** shows the lower resistivity of the blend nanocomposites prepared via PLLA/CNT masterbatch than those prepared via EVA/CNT masterbatch).

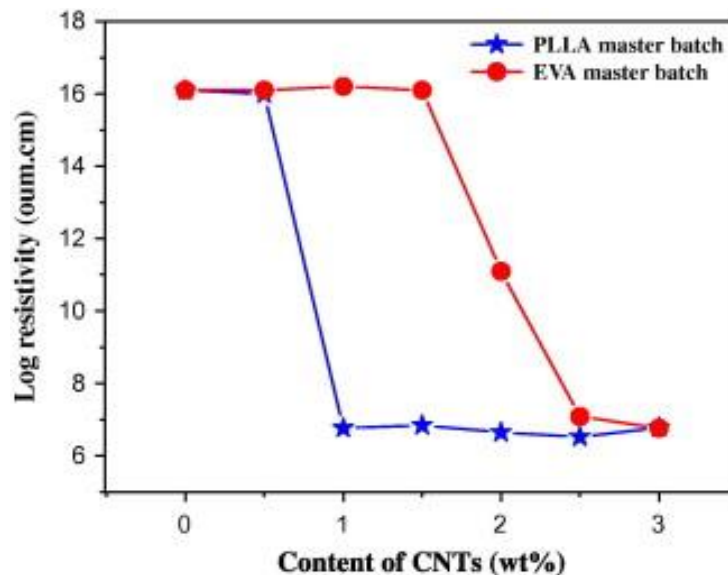


Figure 24. Electrical resistivity of PLLA/EVA/CNT blend as a function of CNT loading prepared via PLLA/CNT and EVA/CNT masterbatch methods^[91] Blend compositing was fixed at (60/40) PLLA/EVA . Copyright 2013. Reproduced with permission from Elsevier Sci. Ltd.

Xu et al.^[90] reported that when MWNTs passed through the interface after 30 min of mixing and were completely accommodated inside the PA6 after migration from the PPS, the resistivity of the final blend nanocomposite increased dramatically relative to when particles were at the interface between PPS and PA6. It was suggested that PA6 droplets were interconnected through the MWNTs at the interface, as illustrated in **Figure 25**, and formed conductive networks while nanocomposites with MWNTs inside the 20 wt. % PA6 were non-conductive since no interconnection existed in such nanocomposites. Similarly, Huang et al.^[180] found 4 min of mixing was sufficient to seize the CNTs at the interface of (50/50) PLA/PCL blend, with melt blending of premixed PLA/CNT and PCL yielding the highest conductivity. This dropped to the lowest conductivity at longer mixing time (8 min) and beyond (as plotted in **Figure 26**) due to the completed migration to the PCL phase. In a different study, Zhao et al.^[112] found that migration of MWNT to the PVDF phase from the PS/MWNT masterbatch takes longer than 30 min with improving electrical conductivity as a function of mixing time. Note that the volume ratio of the polymers were 50/50 and blend composites showed co-continuous morphologies. In their study, blends with MWNTs inside the PVDF phase prepared via PVDF/MWNT masterbatches showed the highest conductivities and dielectric constants, which is believed to be due to the formation of a conductive path through the PVDF phase. This is in contrast with other studies where the highest conductivities were obtained when particles accumulated at the interface, since during the migration there might be some MWNTs at the interface.

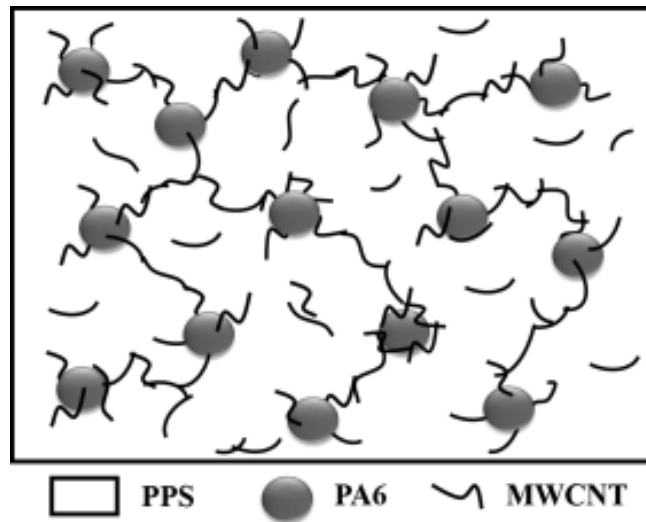


Figure 25. Schematic morphologies of PPS/PA6/MWNT blend nanocomposites prepared via dilution of the PPS/MWNT masterbatch where PA6 is the minor phase ^[90]. Copyright 2015. Reproduced with permission from Wiley-VCH Verlag.

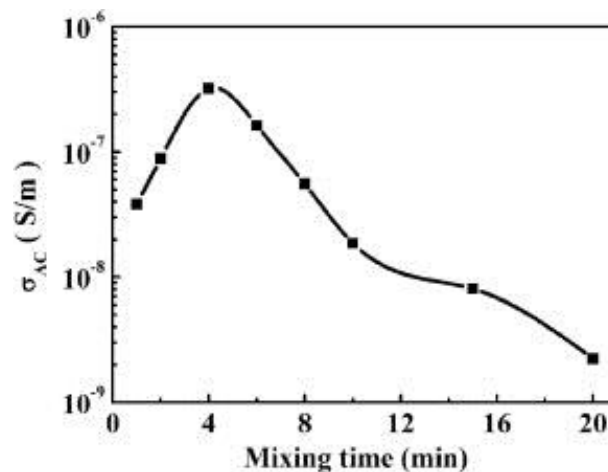


Figure 26. AC conductivity of 0.25 wt%-incorporated (PLA + MWNT)/PCL nanocomposite at different times. ^[180]. Copyright 2014. Reproduced with permission from Elsevier Sci. Ltd.

Chen et al. ^[181] altered the surface of MWNTs by controlling the carboxyl content so that they could be localized at the interface of PMMA/PS blend. It was found that 0.73 wt% was the optimum concentration of carboxyl content for MWNTs to be present at the interface. Interestingly, nanocomposites prepared with this particular functionalization were found to have higher conductivity than those where MWNTs were in the PS or PMMA phase due to effects on the migration of MWNTs to the interface.

Lee et al. ^[40] proposed a “filler-transfer-induced dispersion” mechanism to produce blends with better dispersions when CNTs were pre-dispersed with the less favorable (PS/PPE) phase prior to blending with the more favorable PA66 phase (See **Figure 6**). It was found that

nanocomposites prepared using this method showed lower electrical resistivity than the other sequences where there was no migration involved in the final CNT localization (See **Figure 27**), indicating that migration can bring about better conductivity owing to the improved dispersion. It is worth noting that breaking the nanotubes during melt blending is inevitable which may cause the state of the nanotube dispersion^[144].

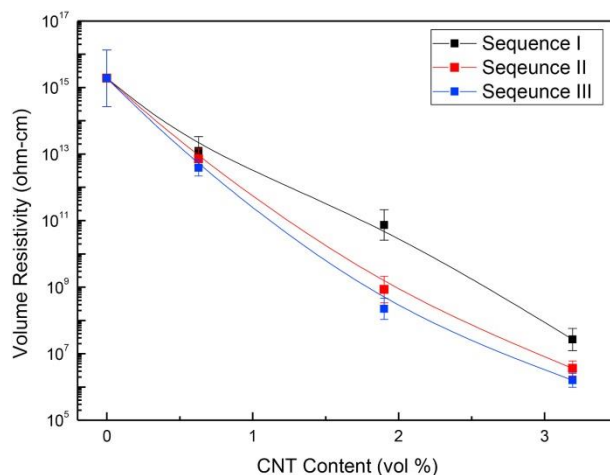


Figure 27. Volume resistivity of the PA66/(PS/PPE)/CNT nanocomposites prepared via simultaneous mixing (Sequence I), PA66/CNT masterbatch (Sequence II), and (PS/PPE)/CNT masterbatch (Sequence III) as a function of CNT concentration^[40]. Copyright 2016. Reproduced with permission from Elsevier Sci. Ltd.

Gong et al.^[93] utilized the same phenomenon to produce homogeneously dispersed ORC/MWNT composites with the assistance of the migration process in such a way that MWNTs were first embedded within the PEO phase (showing individual structures without severe agglomeration) and then blended with ORC (The weight ratio of PEO/ORC was 50/50). Thermodynamic driving forces caused the migration of MWNTs to the more favorable ORC phase. ORC/MWNT composites with uniform dispersion of nanotubes were obtained by etching out the MWNT-free PEO phase after 15 min of blending (See **Figure 7**). The resultant composites were found to have higher conductivity and lower percolation threshold ($10^{-8} < \sigma \text{ (S.m}^{-1}\text{)} < 10^{-6}$ at 0.35 vol. %) than those of the ORC/MWNT composites prepared via conventional single-step melt mixing ($10^{-14} < \sigma \text{ (S.m}^{-1}\text{)} < 10^{-12}$ at 3.82 vol. %). This unique procedure to make uniform nanocomposites is appreciated; however, it would be more helpful if the conductivities of the final co-continuous blend composites were measured before removal of PEO and re-melting of ORC/MWNT to observe the effect of double-percolation structures. It has been previously found that conductivities of double-percolated systems are much higher than those of composites made of each blend's phases^[30, 88, 176].

Gao et al. ^[182] applied the hot stretch technique, similar to what was discussed previously ^[68] (section 6.2), to produce conductive blend nanocomposites of PE/PC/CNT where the weight ratio of PC/PE was fixed at 1/3, as illustrated in **Figure 28**.

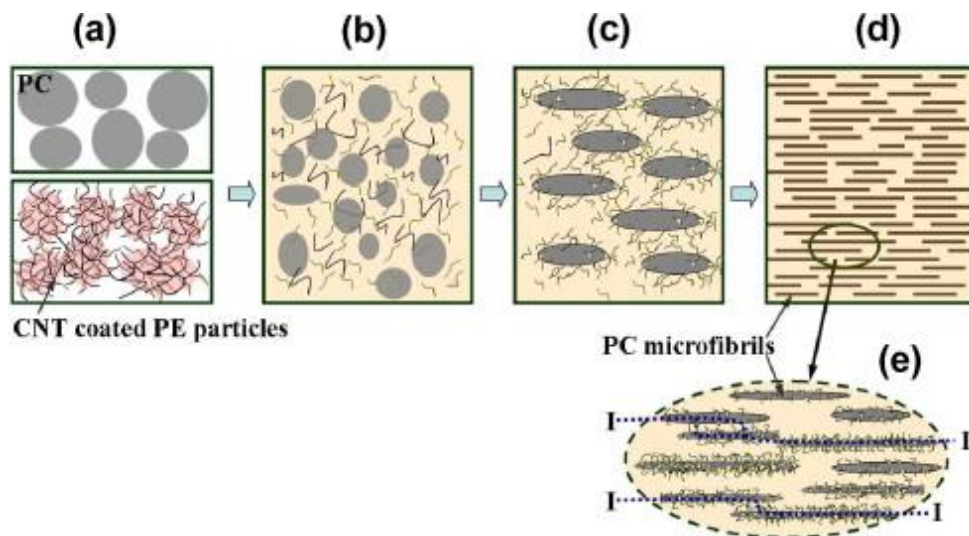


Figure 28. Cartoon illustrating the procedure for making PE/PC/CNT conductive nanocomposite. (a) Mixing CNT-coated PE and PC before blending, (b) blending CNT-coated PE and PC, (c) starting the migration of CNTs from the PE phase to PC during stretching, and (d, e) production of conductive blends from PC microfibrils upon further stretching in a PE matrix ^[182]. Weight ratio of the PC/PE was kept at 1/3. Copyright 2010. Reproduced with permission from Elsevier Sci. Ltd.

In agreement with other studies, it was reported that the hot stretching method is an industrially feasible way to yield a conductive blend nanocomposite. Further, they found the anisotropic conductivity where the volume resistivity of the nanocomposite was a function of stretching reaction and direction, as shown in **Figure 29**.

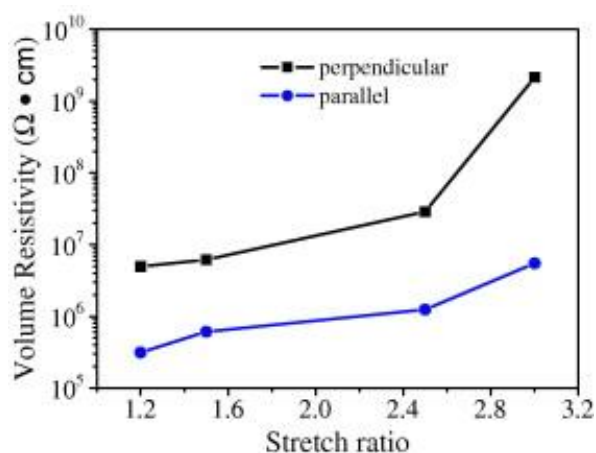


Figure 29. Volume resistivity of PE/PC/CNT blend nanocomposite as a function of stretch ratio parallel and perpendicular to the stretch direction ^[182]. Copyright 2010. Reproduced with permission from Elsevier Sci. Ltd.

The important role of migration in immiscible polymer blends is stressed here. It is clear that preparing polymer blend nanocomposites with CNTs localized at the interface using a two-step process (CNT masterbatch or pre-compounded with thermodynamically disfavored phase) benefits the migration process to help disperse them evenly at the interface. This was shown to be more effective in enhancing the electrical properties than blends prepared from a single-step (simultaneously mixed) method.

6.4. Reduced Graphene oxide

Recently, Bai et al. ^[37] studied the effect of r-GO localization on the electrical conductivity and structure-properties of the PLA/PS blends. In order to obtain the co-continuous morphology the volume ratio of PLA/PS was kept at 48/52. The r-GO sheets were pre-compounded separately with either PLA or PS; the obtained composites were blended with the other virgin polymer. r-GO was found to be thermodynamically more stable in PS due to strong π - π interaction with PS, though r-GO sheets were trapped at the interface during blending due to minimum free energy obtained at this stage. It was revealed that conductivity, morphological stability, and modulus of the blends prepared via PLA/r-GO pre-compounding increased due to the formation of a network as r-GO migrated from PLA to the interface during annealing (**Figure 30**). Further, the blends prepared via (PLA/r-GO)/PS demonstrated higher conductivities than blends prepared via (PS/r-GO)/PLA, with an extreme low percolation threshold of 0.028 vol%.

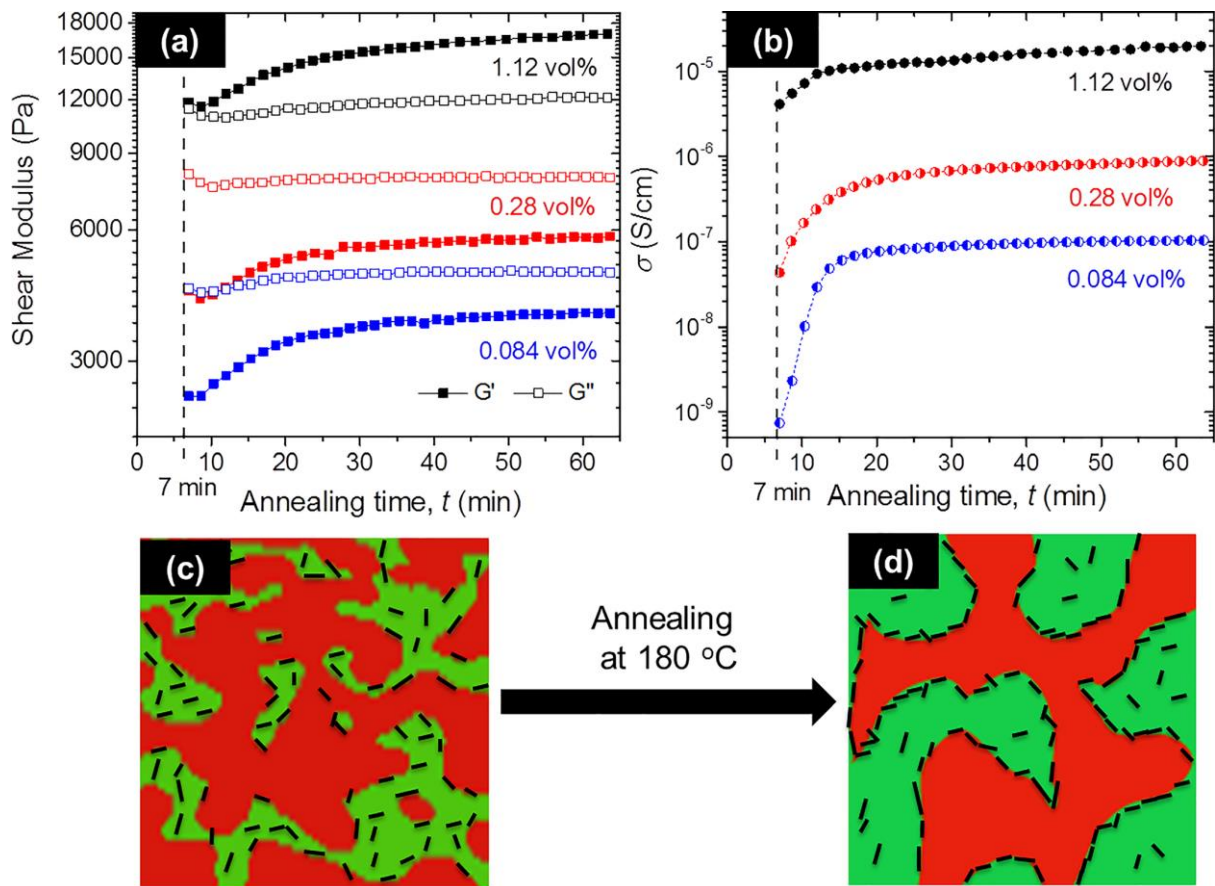


Figure 30. (a) Storage (G') and loss (G'') moduli of (PLA/r-GO)/PS blends at different concentrations of r-GO as a function of annealing time at 180 °C, measured at frequency of 1 rad/s and strain of 1%. (b) Electrical conductivity of the corresponding blends at $\omega_{AC} = 20$ Hz simultaneously taken with rheological properties as a function of annealing time. Cartoon illustrating the interfacial localization of r-GO (c) at the early stage of annealing (~7 min) and (d) after ~30 min of annealing (where morphology is stabilized). Red and green regions represent PS and PLA phases respectively^[37]. Copyright 2017. Reproduced with permission from The Society of Rheology.

6.5. Hybrid effect

A unique approach to achieve a low percolation threshold is using the synergistic effect of hybrid nanocomposites^[183]. Pötschke et al.^[184] proposed to use a hybrid polymer blend system PP+MMT/PC+MWNT to avoid migration toward the undesired phase. In this case, the co-continuous morphology was achieved when the weight percentage of the filled PC was between 40 and 80 vol%. The final goal was to use MWNT at the lowest amount possible to reach the highest conductivity for PC/PP blends. To achieve such a behavior, CNTs had to remain in the PC as it was previously found that their migration toward the other (PE) reduced the conductivity in a PC/PE blend where co-continuous morphologies were found to be in a range of 30 to 80 vol.% of the filled PC^[185]. Therefore, the blends of PC/MWNT and PP/MMT were tailored in a way to obtain the co-continuous morphology. MMT was used as a shield to prevent MWNT migration toward the PP phase by localizing at the interface between PC and PP, as shown in **Figure 31**. It

was revealed that blends prepared by that method show significant conductivity with only 0.6 vol% of MWNT.

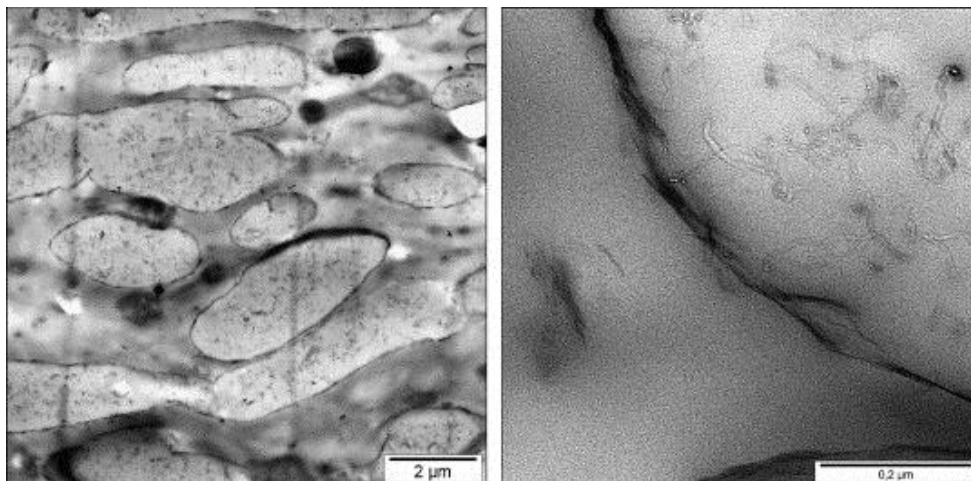


Figure 31. TEM images of (60/40) wt. % of PP + MMT/PC + CNT blends ^[184]. Copyright 2007. Reproduced with permission from Elsevier Sci. Ltd.

Chen et al. ^[186] similarly utilized GO particles to trap CNTs at the interface of (60/40) PLLA/EVA blend to enhance the electrical conductivity of the blend at a very low percolation threshold.

Figure 32 represents the schematic mechanisms for trapping CNTs at the interface by introducing GO particles.

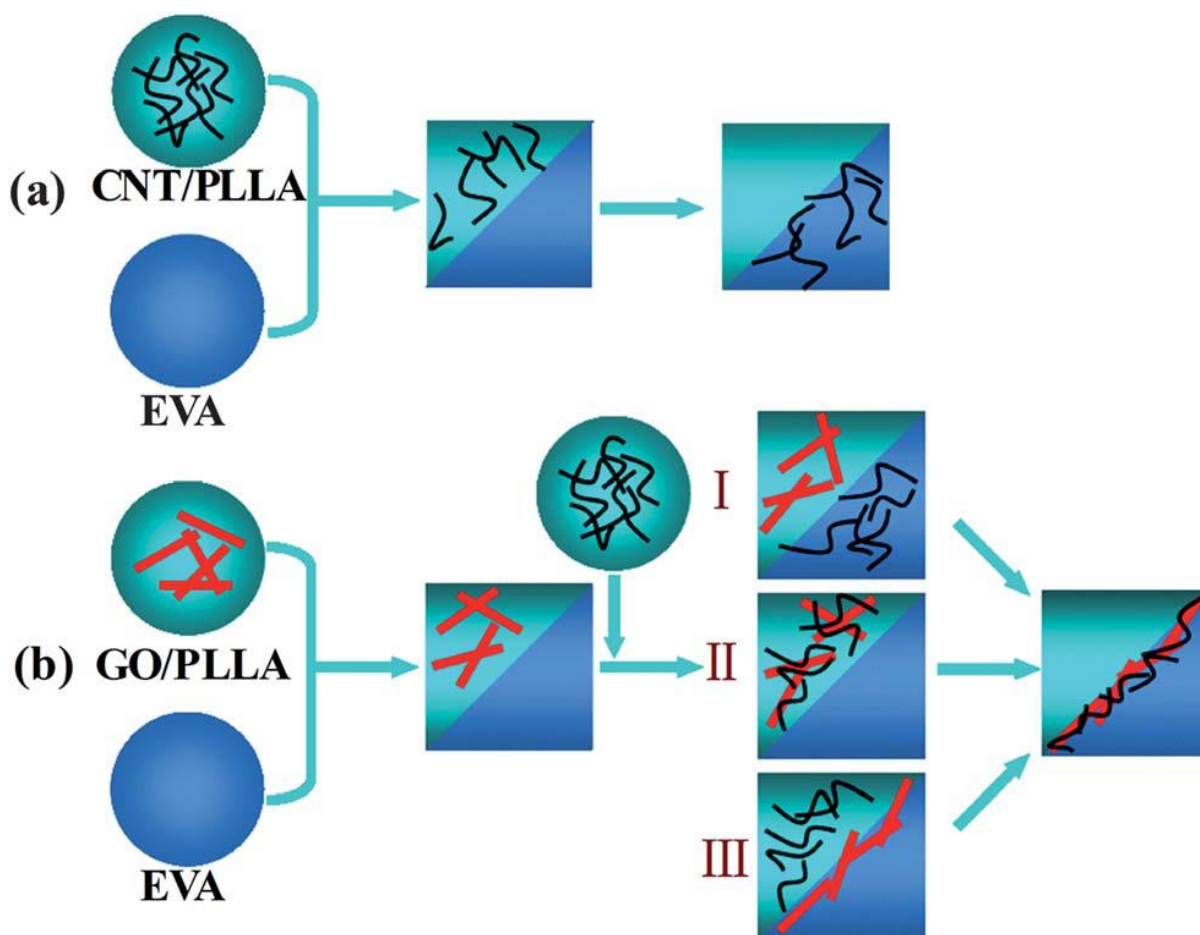


Figure 32. Schematic view of CNT localization at the interface of (60/40) PLLA/EVA blend. Preparation of (a) PLLA/EVA/CNT and (b) PLLA/EVA/CNT/GO blend nanocomposites. Concentrations of CNT and GO were 0.1 and 0.3 wt%, respectively ^[186]. Copyright 2013. Reproduced with permission from The Royal Society of Chemistry.

Three different possibilities were proposed for trapping CNTs at the interface by GO incorporation, as illustrated in **Figure 32(b)**. (I) Interfacially localized GO particles attract CNTs from the PLLA phase to the interface due to π - π interactions. (II) A GO/CNT complex is formed during the initial compounding stages and both migrate to the interface. (III) GO particles at the interface act as a shield to keep CNTs at the interface from migrating to the EVA phase. Interestingly, PLLA/EVA/CNT/GO blends exhibited significant reduction of about 7 order of magnitude to ($10^7 \Omega \cdot \text{m}$) in volume resistivity compared to those blends filled with only CNT or GO, as shown in **Figure 33**.

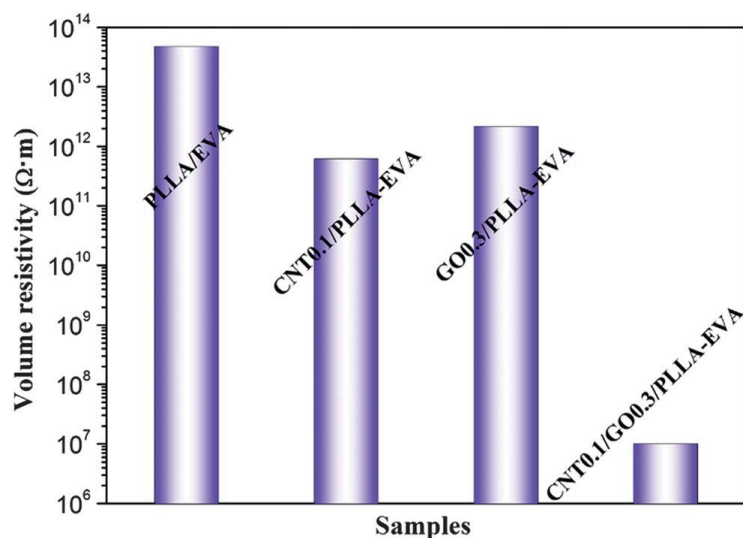


Figure 33. Volume resistivity of the co-continuous (60/40) PLLA/EVA blends incorporated with CNT, GO, and CNT/GO complex ^[186]. Copyright 2013. Reproduced with permission from The Royal Society of Chemistry.

The same authors ^[187] reported that organoclays at 0.1 wt% can be used in (40/60) PC/PVDF blends to trap CNTs at the interface. The aim was to have CNT particles at the interface knowing that they have higher tendency to localize in the PC phase. Hence, organoclays were used to act as a shield to prevent the migration of CNTs from PVDF/CNT masterbatch toward the PC/clay phase, similar to the work of Pötschke et al. ^[184]. It was found that the amount of CNTs trapped at the interface (and in turn the conductivity) is a function of concentrations of both organoclay and CNT with both concentrations increasing the CNT at the interface and decreasing conductivity. Later, the percolation threshold for CNT concentration was found to be 0.06 wt%, the same as in their previous work ^[186].

The above results reveal that accommodating nanotubes at the interface is a key factor to obtain the lowest electrical resistivity (the best electrical conductivity). This requires altering the blending strategy, mixing time, or modification of particles.

Table 6 summarizes the findings, in which the influence of particle migration in blends prepared through different techniques and mixing order, on electrical properties of the corresponding blends.

Table 6. Summary of the literature findings in which the particle migrations affected the electrical properties of the blends with regard to their mixing order. All the references used melt mixing process.

Blending order	Polymer composition	ϕ [filler]	Final localization (experimental)	Final localization (estimated)	Migration-induced conductivity
(PMMA+ ϕ)/PS PMMA/(PS+ ϕ) ^[65] PMMA/PS/ ϕ	(PMMA/PS) (50/50) vol%	Carbon black Printex XE2 (Evonik Rohm)	PS	PS ^a	No significant changes in electrical conductivity for different protocols $10^{-5} < \sigma [S\ cm^{-1}] < 10^{-3}$
(PP+PA)/ ϕ (PP+ ϕ)/PA ^[64] PP/(PA+ ϕ)	Table 5	Carbon black Ketjenblack EC (Akzo)	PA	N/A	Fast migration from PP to PA. Lowest resistivity obtained when CB migrated from PA minor phase and it decreased with increasing CB content [Resistivity $\cong 10^4$ ohm cm].
(PS+PIP)/ ϕ ^[178]	(PS/PIP) (45/55) vol%	Carbon black BP2000 (CABOT) And XE2 (Degusa)	Interface	N/A	Lowest electrical resistivity obtained when particles at the interface of co-continuous (45/55) PS/PIP blend. [Resistivity $\cong 10^2$ and 10^3 ohm cm for 1.5 and 1.2 vol% of XE2 and BP2000 CB, respectively]
(PS+ ϕ)/PE PS/(PE+ ϕ) ^[66]	(PE/PS) (45/55) wt. %	Carbon black	Varied depending on mixing time	N/A	CB particles migrated to interface from PS within 2 min of mixing with the percolation threshold of 0.4 wt%. The lowest electrical resistivity was obtained at 10 wt% of CB at the interface [Resistivity $< 10^1$ ohm cm].
(PS+ ϕ)/PE PS/(PE+ ϕ) ^[69]	(PE/PS) (45/55) wt. %	Carbon black BP1000 (CABOT) and XE2 (Degusa)	Varied depending on mixing time	N/A	XE2 CB particles migrated faster from PS (2 min) to the interface and were less stable at the interface than BP100 CB (3.5–5 min) with minimum electrical resistivity of $\approx 10^4$ and 10^5 ohm cm respectively.
(PET+ ϕ)/PE PET/PE/ ϕ ^[67]	(PET/PE) (30/70) wt. %	Carbon black			Hot stretch method via extrusion through a slit die was

		MZ (National Chemical CO. Ningxia, China)	PET	N/A	<i>used to prepare PET microfibrils via PET/CB pre-mixtures. Low percolation threshold was obtained for the hot stretched samples [3/7 vol%] with $10^5 < \text{Resistivity [ohm cm]} < 10^6$</i>
(PET+φ)/PE [68]	(PET/PE) (1/3.2) vol. %	Carbon black MZ from (China) and Carbon black VXC-605 (CABOT)	PET and partially interface	N/A	<i>MZ carbon black resulted in lower percolation threshold [Li2004].</i>
(PE+φ)/PET PE/PET/φ [71]	(PET/PE) (1/3.2) vol. %	Carbon black VXC-605 (CABOT)	Interface and PET(in direct mixing method)	PET ^b	<i>CB migrated to the surface of PET microfibrils during hot stretching and caused a lower percolation threshold [3.8 vol%] than the direct method with electrical resistivity of $\approx 10^8$ ohm cm respectively.</i>
(PC+φ)/SAN PC/(SAN+φ) [88] PC/SAN/φ	(PC/SAN) (60/40) wt. %	MWNT C150HP (Bayer MaterialScience AG)	PC	PC ^a	<i>Nanotubes migrated within 5 min from SAN to PC. Final volume resistivity of the blends were similar, irrespective of their blending protocols $10^2 < \text{Resistivity [ohm cm]} < 10^4$</i>
(PE+ φ)/PA6 (PE+ φ)/PC [92]	PE was 0.32 wt. % at 44 wt. % MWNT	MWNT Nanocyl [®] -9000 (Nanocyl S.A., Belgium)	PA6 and PC	PA6 and PC	<i>High density PE with high MWNT content was synthesized and introduced into the PA6 or PC as nanotube carriers to improve the dispersion of MWNTs inside the matrix. Almost all of the MWNTs migrated to the PA6 or PC matrix during the melt blending leading to a dispersion of separate nanotubes in the matrix without agglomerations. The resistivity of lower than 10^4 ohm cm was achieved for the blend with incorporation of PE/MWNT concentrates into the PA6 or PC.</i>
(PC-RC+φ)/SAN (SAN+φ)/PC-RC [179] PC-RC/SAN/φ	(SAN/PC) (40/60)	Short amino functionalized MWNT Nanocyl TM NC3152 (Nanocyl S.A.,	SAN	N/A	<i>The reactive component RC changed the location of MWNTs from PC to SAN while destroying the conductivity. Resistivity [ohm cm] $\sim 10^{16}$</i>

Belgium)					
(PA+φ)/PE PA/(PE+φ) [26] PA/PE/φ	(PE/PA) (75/25), (50/50) and (25/75) wt. %	MWNT Nanocyl®-7000 (Nanocyl S.A., Belgium)	interface and PA	N/A	<i>Nanotubes remained inside PA phase when they were premixed with PA. Blends prepared via premix with PE had lower resistivity when PE was minor phase.</i>
(PPS+φ)/PA6 PPS/PA6/φ [90]	(PPS/PA6) (90/10), (80/20) and (70/30) wt. % for masterbatch method	MWNT (Tsinghua University, China)	PA6 And partially interface	PA6 ^a	<i>Lowest electrical resistivity obtained at PA6 concentrations of 40-90 wt% and 10-90 wt% for the direct and masterbatch methods, respectively $\approx 10^3$ ohm cm. Slow migration of nanotubes from PPS to PA6 after 30 min of mixing resulted in significant increase in electrical resistivity [$\approx 10^{10}$ ohm cm] due to destruction of the interconnected network.</i>
(PE+φ)/PC [182]	(PC/PE) (1/3) wt. %	MWNT (Chengdu Organic Chemicals, Ltd., China)	interface	PC ^c	<i>Hot stretch method via extrusion through a slit die was used to promote the migration from PE to the microfibrillar PC surface. The lowest volume resistivity was obtained at the stretch ratio of 1.2, parallel to the stretch direction $10^5 < \text{Resistivity [ohm cm]} < 10^6$</i>
PLLA/(EVA+φ) (PLLA+φ)/EVA [91]	(PLLA/EVA) (60/40) wt. %	MWNT (Chengdu Organic Chemicals, Ltd., China)	EVA And interface	PLLA ^a	<i>Blends of PLLA/MWNT masterbatch method resulted in nanotubes at the interface with lower electrical resistivity of nearly 10^7 ohm cm.</i>
(PLA+φ)/PCL [180]	(PLA/PCL) (50/50) wt. %	MWNT (Chengdu Organic Chemicals, Ltd., China)	Varied depending on the mixing time	N/A	<i>After 4 min of mixing, particles were at the interface and further mixing led the nanotubes to move to the PCL phase resulting in decreased electrical conductivity at longer times. The highest conductivity was obtained at 1.5 wt% of nanotubes and at 4 min of mixing $\sigma [S m^{-1}] \sim 10^{-3}$</i>

(PS+φ)/PVDF PS/(PVDF+φ)^[112] PS/PVDF/φ	(PS/PVDF) (1/1) vol. %	MWNT (Shenzhen Nanotech Co.,) Port	PVDF and partially PS	PVDF ^a	<i>Long (more than 30 min) migration process from PS to PVDF. Blends prepared from PVDF/MWNT showed higher electrical conductivities.</i>
((PS/PPE)+φ)/PA66 (PS/PPE)/(PA66+φ)^[40] (PS/PPE)/PA66/φ	(PA6/(PS/PPE) (60/40) wt. %	MWNT Nanocyl [®] -7000 (Nanocyl S.A., Belgium)	PA66	PA66 ^a	<i>Quick migration of nanotubes from PS/PPE to PA66 within 60 s. Dispersion of nanotubes in PA66 were better when they premixed with PS/PPE initially. Blends prepared from (PS/PPE)/CNT masterbatch showed the lowest resistivity of nearly 10⁶ ohm cm at 3.2 vol% of CNT.</i>
(PLA+φ)/PS (PS+φ)/PLA^[37] PLA/PS/φ	(PLA/PS) (48/52) vol. %	Synthesized Graphene oxide	PS and interface (in PLA/GO masterbatch)	PS ^c	<i>Ultralow percolation threshold of 0.028 vol% was obtained in blends prepared from PLA/GO masterbatch due to the GO sheets trapped at the interface during migration. A correlation between rheological network and electrical conductivities was proposed.</i>

a= Calculations based on Eq. (2, 3); b= Calculation based on Eq. 3; c= Calculations based on Eq.2.
Brackets in the blending order indicate the premixtures.

7. Conclusions and Future outlook

The role of nanoparticles in polymer blends as compatibilizers or conductivity boosters has already been discussed in many articles and book chapters. It can be understood that melt blending is an attractive method for fabricating conductive polymer nanocomposites due to its potential in mass production. Further, it was stated that the multiphase structure in immiscible blends could be utilized for tuning the final properties with respect to the structure and strength of the conductive network. Such a conductive network was found to be directly dependent on the localization of the particles within the polymer blend. The particle distribution can be significantly affected by many thermodynamic and kinetic parameters such as interfacial tensions, blending sequence, mixing time and polymer pair's viscosities. Interfacial localization of the particles have been extensively reported to be the key issue in having the best electrical properties, and many efforts have been made to achieve such localizations. The most efficient strategy is using a mixing sequence whereby the particles are pre-dispersed in the disfavored component to stimulate the migration process to the favored phase. Thus by stopping the process at the right time, the interfacially localized distributions could be attained.

This paper merely discussed the mechanisms involved in the migration of nanoparticles within polymer blends considering the different external factors influencing the kinetics of migration and in turn, the influences that migration can have on the conductivity of the final blend. It was found that despite the tendency of particles to accumulate in the thermodynamically preferred component, it is possible to manipulate this tendency by modifying some parameters at processing levels or material modifications. Such a process requires a fair amount of applied force and time to complete the migration. Another parameter that can facilitate the migration process is the surface modification of nanoparticle with moieties more attracted to the other component, the right selection of nanoparticles with respect to geometry (particles with larger aspect ratios migrate faster), and changing the viscosity ratio. Generally, a chain of requisite parameters (thermodynamic and kinetics) is involved in the migration of nanoparticles from one component to the other where none can be disregarded. This makes the whole migration process and mechanisms associated with it quite complex where a lack of any of the hitherto discussed parameters can impede the migration. Especially when in practice these particles are dispersed in form of clusters and their orientation inside the primary component and at the interface, play an important role in the rate of migration.

Now the question is, “Why all these manipulations?” The answer was found in different properties achieved when compared to conventional blend composites, where there was no indication of migration. An outstanding response to this was the significant influence on electrical conductivity of the blends. It was found that immiscible blends with nanoparticles at the interface have the best conductivities with low percolation threshold by forming a network of interconnected particles throughout the blend ^[188]. Interestingly, it was revealed that those blends with nanoparticles that migrated to the interface in sequential blending methods showed higher conductivities than those with nanoparticles at the interface from a single-step blending method ^[189]. That is, migration can play an irrefutable role in the distribution and dispersion of nanoparticles. With this knowledge, it will be interesting to study the influence of nanotube structures (e.g., multi-walled, double-walled, and single-walled) on the kinetics of migration and its effect on properties such as the electrical and thermal conductivities. Graphene-based particles are another class of particles that deserve a fair amount of study of their migration.

It can be inferred that carbon blacks have been more commonly used due to cost-related issues compared with other more expensive conductive nanoparticles particles such as graphene or nanotubes, the latter with growing trends. However, close inspection of the current search with nanoparticles having conductive characteristics reveals that CNTs and graphene dominate with graphene as a new emerging carbon-based nanomaterial growing very fast in this chart due to its superior electrical and thermal conductivities (exceeding those of CNTs) and outstanding enhancements in mechanical properties.^[94, 190, 191] It has been discussed that graphene-based materials are better candidate for electronic devices as the heating from high resistance is lower than that of CNT. Moreover, graphene-based polymer nanocomposites exhibit higher power conversion efficiency (PCE) than CNT-based polymer nanocomposites, which makes them a good candidate for solar cell applications ^[192].

Acknowledgment.

The authors would like to thank the Department of Science and Technology (HGERA8X) and the Council for Scientific and Industrial Research (HGER74P), South Africa for financial support. We also sincerely thank Editors for invitation and reviewers for valuable and insightful comments. Furthermore, the authors thank Miss Margaret Ward for manuscript proof reading.

References

- [1] [1a] S.S. Ray, *Polymer* **2010**, *51*, 3966. [1b] S. S. Ray, Clay-Containing Polymer Nanocomposites. From Fundamentals to Real Applications, 1st Edition; Elsevier: Oxford, **2013**. [1c] S. S. Ray, M. Okamoto, *Prog. Polym. Sci.* **2003**, *28*, 1539.
- [2] M. M. Rueda, M.-C. Auscher, R. Fulchiron, T. Périé, G. Martin, P. Sonntag, P. Cassagnau, *Prog. Polym. Sci.* **2017**, *66*, 22.
- [3] J. Bandyopadhyay, S. S. Ray, *Inorganic Nanosheets and Nanosheet-Based Materials: Fundamentals and Applications of Two-Dimensional Systems* **2017**, 501.
- [4] A. Gupta, T. Sakthivel, S. Seal, *Prog. Mater.Sci.* **2015**, *73*, 44.
- [5] J.-M. Thomassin, C. Jerome, T. Pardoen, C. Bailly, I. Huynen, C. Detrembleur, *Mater. Sci. Eng., R* **2013**, *74*, 211.
- [6] P. K. S. Mural, S. P. Pawar, S. Jayanthi, G. Madras, A. K. Sood, S. Bose, *ACS Appl. Mater. Interfaces.* **2015**, *7*, 16266.
- [7] Z.-M. Dang, J.-K. Yuan, J.-W. Zha, T. Zhou, S.-T. Li, G.-H. Hu, *Prog. Mater.Sci.* **2012**, *57*, 660.
- [8] R. A. Antunes, M. C. L. de Oliveira, G. Ett, V. Ett, *J. Power Sources* **2011**, *196*, 2945.
- [9] Q. Wang, T. Wang, J. Wang, W. Guo, Z. Qian, T. Wei, *Polym. Adv. Technol.* **2018**, *29*, 407.
- [10] T. Villmow, S. Pegel, A. John, R. Rentenberger, P. Pötschke, *Mater. Today* **2011**, *14*, 340.
- [11] Y. Kato, M. Horibe, S. Ata, T. Yamada, K. Hata, *RSC Adv.* **2017**, *7*, 10841.
- [12] M. Salzano de Luna, G. Filippone, *Eur. Polym. J.* **2016**, *79*, 198.
- [13] A. E. Nesterov, Y. S. Lipatov, *Polymer* **1999**, *40*, 1347.
- [14] S. S. Ray, S. Pouliot, M. Bousmina, L. A. Utracki, *Polymer* **2004**, *45*, 8403.
- [15] H. Wang, C. Zeng, M. Elkovitch, L. J. Lee, K. W. Koelling, *Polym. Eng. Sci.* **2001**, *41*, 2036.
- [16] Y. Yoo, C. Park, S.-G. Lee, K.-Y. Choi, D. S. Kim, J. H. Lee, *Macromol. Chem. Phys.* **2005**, *206*, 878.
- [17] J. Huitric, J. Ville, P. Médéric, M. Moan, T. Aubry, *J. Rheol.* **2009**, *53*, 1101.
- [18] M. Trifkovic, A. T. Hedegaard, M. Sheikhzadeh, S. Huang, C. W. Macosko, *Macromolecules* **2015**, *48*, 4631.
- [19] R. Salehiyan, H. Y. Song, M. Kim, W. J. Choi, K. Hyun, *Macromolecules* **2016**, *49*, 3148.
- [20] S. S. Ray, M. Bousmina, *Macromol. Rapid Commun.* **2005**, *26*, 1639.
- [21] Y. S. Lipatov, A. E. Nesterov, T. D. Ignatova, D. A. Nesterov, *Polymer* **2002**, *43*, 875.
- [22] J. Vermant, G. Cioccolo, K. Golapan Nair, P. Moldenaers, *Rheol. Acta* **2004**, *43*, 529.
- [23] S. Vandebriel, J. Vermant, P. Moldenaers, *Soft Matter* **2010**, *6*, 3353.
- [24] D. Wu, D. Lin, J. Zhang, W. Zhou, M. Zhang, Y. Zhang, D. Wang, B. Lin, *Macromol. Chem. Phys.* **2011**, *212*, 613.
- [25] F. Tao, D. Auhl, A.-C. Baudouin, F. J. Stadler, C. Bailly, *Macromol. Chem. Phys.* **2013**, *214*, 350.
- [26] L. Zonder, A. Ophir, S. Kenig, S. McCarthy, *Polymer* **2011**, *52*, 5085.
- [27] R. Salehiyan, S. Sinha Ray, *Macromol. Materi. Eng.* **2018**, *303*, 1800134.
- [28] A. Taguet, P. Cassagnau, J. M. Lopez-Cuesta, *Prog. Polym. Sci.* **2014**, *39*, 1526.
- [29] S. Bose, C. Özdilek, J. Leys, J. W. Seo, M. Wübberhorst, J. Vermant, P. Moldenaers, *ACS Appl. Mater. Interfaces.* **2010**, *2*, 800.
- [30] M. Sumita, K. Sakata, S. Asai, K. Miyasaka, H. Nakagawa, *Polym. Bull.* **1991**, *25*, 265.
- [31] S. Wu, "Polymer interface and adhesion", M. Dekker, 1982.
- [32] N. R. Demarquette, A. M. C. De Souza, G. Palmer, P. H. P. Macaubas, *Polym. Eng. Sci.* **2003**, *43*, 670.

- [33] D. K. Owens, R. C. Wendt, *J. Appl. Polym. Sci.* **1969**, *13*, 1741.
- [34] A.-C. Baudouin, J. Devaux, C. Bailly, *Polymer* **2010**, *51*, 1341.
- [35] A. Taghizadeh, B. D. Favis, *Carbohydr. Polym.* **2013**, *98*, 189.
- [36] E. Jalali Dil, B. D. Favis, *Polymer* **2015**, *76*, 295.
- [37] L. Bai, S. He, J. W. Fruehwirth, A. Stein, C. W. Macosko, X. Cheng, *J. Rheol.* **2017**, *61*, 575.
- [38] L. Elias, F. Fenouillot, J. C. Majesté, G. Martin, P. Cassagnau, *J. Polym. Sci., Part B: Polym. Phys.* **2008**, *46*, 1976.
- [39] F. Chinesta, G. Ausias, "*Rheology of Non-spherical Particle Suspensions*", Elsevier, 2015.
- [40] C. J. Lee, R. Salehiyan, D. S. Ham, S. K. Cho, S.-J. Lee, K. J. Kim, Y. Yoo, K. Hyun, J. H. Lee, W. J. Choi, *Polymer* **2016**, *84*, 198.
- [41] H. Yoon, K. Okamoto, M. Yamaguchi, *Carbon* **2009**, *47*, 2840.
- [42] V. A. Doan, S. Nobukawa, S. Ohtsubo, T. Tada, M. Yamaguchi, *J. Polym. Res.* **2013**, *20*, 145.
- [43] R. Wiwattanankul, Y. Hachiya, T. Endo, S. Nobukawa, M. Yamaguchi, *Composites, Part B* **2015**, *78*, 409.
- [44] J. S. Hong, Y. K. Kim, K. H. Ahn, S. J. Lee, *J. Appl. Polym. Sci.* **2008**, *108*, 565.
- [45] M. Nofar, M. C. Heuzey, P. J. Carreau, M. R. Kamal, *Polymer* **2016**, *98*, 353.
- [46] P. Thareja, K. Moritz, S. S. Velankar, *Rheol. Acta* **2010**, *49*, 285.
- [47] S. Nagarkar, S. S. Velankar, *J. Rheol.* **2013**, *57*, 901.
- [48] S. P. Nagarkar, S. S. Velankar, *Soft Matter* **2012**, *8*, 8464.
- [49] P. Thareja, S. Velankar, *Rheol. Acta* **2008**, *47*, 189.
- [50] Z.-M. Zou, Z.-Y. Sun, L.-J. An, *Rheol. Acta* **2014**, *53*, 43.
- [51] A. Gödel, A. Marmur, G. R. Kasaliwal, P. Pötschke, G. Heinrich, *Macromolecules* **2011**, *44*, 6094.
- [52] A. Maani, P. J. Carreau, *J. Non-Newtonian Fluid Mech.* **2016**, *233*, 95.
- [53] S. S. Ray, S. Pouliot, M. Bousmina, L. A. Utracki, *Polymer* **2004**, *45*, 8403.
- [54] A. Dasari, Z.-Z. Yu, Y.-W. Mai, *Polymer* **2005**, *46*, 5986.
- [55] L. T. Vo, E. P. Giannelis, *Macromolecules* **2007**, *40*, 8271.
- [56] J. Xiao, Y. Hu, H. Lu, Y. Cai, Z. Chen, W. Fan, *J. Appl. Polym. Sci.* **2007**, *104*, 2130.
- [57] C. G. Martins, N. M. Larocca, D. R. Paul, L. A. Pessan, *Polymer* **2009**, *50*, 1743.
- [58] A. Bigdeli, H. Nazockdast, A. Rashidi, M. E. Yazdanshenas, *J. Macromol. Sci., Part B* **2016**, *55*, 732.
- [59] J. S. Borah, N. Karak, T. K. Chaki, *Mater. Sci. Eng.* **2011**, *528*, 2820.
- [60] R. Salehiyan, W. J. Choi, J. H. Lee, K. Hyun, *Korea-Aust. Rheol. J.* **2014**, *26*, 311.
- [61] C. Journet, S. Moulinet, C. Ybert, S. T. Purcell, L. Bocquet, *EPL (Europhys. Lett.)* **2005**, *71*, 104.
- [62] D. Y. Kwok, A. W. Neumann, *Adv. Colloid Interface Sci.* **1999**, *81*, 167.
- [63] N. Tsubokawa, *Progress in Polymer Science* **1992**, *17*, 417.
- [64] R. Tchoudakov, O. Breuer, M. Narkis, A. Siegmann, *Polym. Eng. Sci.* **1996**, *36*, 1336.
- [65] S. L. Scherzer, E. Pavlova, J. D. Esper, Z. Starý, *Compos. Sci. Technol.* **2015**, *119*, 138.
- [66] F. Gubbels, R. Jérôme, P. Teyssie, E. Vanlathem, R. Deltour, A. Calderone, V. Parente, J.-L. Brédas, *Macromolecules* **1994**, *27*, 1972.
- [67] Z.-M. Li, X.-B. Xu, A. Lu, K.-Z. Shen, R. Huang, M.-B. Yang, *Carbon* **2004**, *42*, 428.
- [68] X.-B. Xu, Z.-M. Li, M.-B. Yang, S. Jiang, R. Huang, *Carbon* **2005**, *43*, 1479.
- [69] F. Gubbels, R. Jerome, E. Vanlathem, R. Deltour, S. Blacher, F. Brouers, *Chem. Mater.* **1998**, *10*, 1227.
- [70] X.-B. Xu, Z.-M. Li, K. Dai, M.-B. Yang, *Appl. Phys. Lett.* **2006**, *89*, 032105.
- [71] K. Dai, X.-B. Xu, Z.-M. Li, *Polymer* **2007**, *48*, 849.

- [72] J. Suehiro, G. Zhou, M. Hara, *Sens. Actuators, B* **2005**, *105*, 164.
- [73] A. Fujiwara, K. Ishii, H. Suematsu, H. Kataura, Y. Maniwa, S. Suzuki, Y. Achiba, *Chem. Phys. Lett.* **2001**, *336*, 205.
- [74] X. Zhang, H. Cui, Y. Gui, J. Tang, *Nanoscale Res. Lett.* **2017**, *12*.
- [75] J. A. Rodríguez-González, C. Rubio-González, C. A. Meneses-Nochebuena, P. González-García, L. Licea-Jiménez, *Compos. Interfaces* **2017**, *24*, 883.
- [76] S. Liu, G. Wu, Y. Xiao, *Compos. Interfaces* **2017**, *24*, 743.
- [77] R. D. Farahani, J. E. Klemberg-Sapieha, D. Therriault, *Mater. Des.* **2015**, *88*, 1175.
- [78] X. Zhang, X. Yan, Q. He, H. Wei, J. Long, J. Guo, H. Gu, J. Yu, J. Liu, D. Ding, L. Sun, S. Wei, Z. Guo, *ACS Appl. Mater. Interfaces.* **2015**, *7*, 6125.
- [79] S. J. Tans, A. R. M. Verschueren, C. Dekker, *Nature* **1998**, *393*, 49.
- [80] M. V. Kharlamova, *Prog. Mater. Sci.* **2016**, *77*, 125.
- [81] E. Pop, D. Mann, Q. Wang, K. Goodson, H. Dai, *Nano Lett.* **2006**, *6*, 96.
- [82] Y. Li, Z. Zhang, X. Li, J. Zhang, H. Lou, X. Shi, X. Cheng, H. Peng, *J. Mater. Chem. C* **2017**, *5*, 41.
- [83] Q. Cao, J. A. Rogers, *Adv. Mater.* **2009**, *21*, 29.
- [84] C. Li, E. T. Thostenson, T.-W. Chou, *Compos. Sci. Technol.* **2008**, *68*, 1227.
- [85] E. Laredo, M. Grimau, A. Bello, D. F. Wu, Y. S. Zhang, D. P. Lin, *Biomacromolecules* **2010**, *11*, 1339.
- [86] A.-C. Baudouin, D. Auhl, F. Tao, J. Devaux, C. Bailly, *Polymer* **2011**, *52*, 149.
- [87] F. Xiang, Y. Shi, X. Li, T. Huang, C. Chen, Y. Peng, Y. Wang, *Eur. Polym. J.* **2012**, *48*, 350.
- [88] A. Gödel, G. Kasaliwal, P. Pötschke, *Macromol. Rapid Commun.* **2009**, *30*, 423.
- [89] A.-C. Baudouin, C. Bailly, J. Devaux, *Polym. Degrad. Stabil.* **2010**, *95*, 389.
- [90] L. Xu, B.-Y. Zhang, Z.-Y. Xiong, Z.-X. Guo, J. Yu, *J. Appl. Polym. Sci.* **2015**, *132*, n/a.
- [91] Y.-y. Shi, J.-h. Yang, T. Huang, N. Zhang, C. Chen, Y. Wang, *Composites, Part B* **2013**, *55*, 463.
- [92] P. Pötschke, S. Pegel, M. Claes, D. Bonduel, *Macromol. Rapid Commun.* **2008**, *29*, 244.
- [93] T. Gong, M.-Q. Liu, H. Liu, S.-P. Peng, T. Li, R.-Y. Bao, W. Yang, B.-H. Xie, M.-B. Yang, Z. Guo, *Polymer* **2017**, *110*, 1.
- [94] T. Kuilla, S. Bhadra, D. Yao, N. H. Kim, S. Bose, J. H. Lee, *Prog. Polym. Sci.* **2010**, *35*, 1350.
- [95] S. V. Morozov, K. S. Novoselov, A. K. Geim, *Phys.-Usp.* **2008**, *51*, 744.
- [96] A. N. Chaika, V. Y. Aristov, O. V. Molodtsova, *Prog. Mater. Sci.* **2017**, *89*, 1.
- [97] S. Gadipelli, Z. X. Guo, *Prog. Mater. Sci.* **2015**, *69*, 1.
- [98] A. Bianco, H.-M. Cheng, T. Enoki, Y. Gogotsi, R. H. Hurt, N. Koratkar, T. Kyotani, M. Monthieux, C. R. Park, J. M. D. Tascon, J. Zhang, *Carbon* **2013**, *65*, 1.
- [99] S. Stankovich, D. A. Dikin, G. H. B. Dommett, K. M. Kohlhaas, E. J. Zimney, E. A. Stach, R. D. Piner, S. T. Nguyen, R. S. Ruoff, *Nature* **2006**, *442*, 282.
- [100] G. Carotenuto, V. Romeo, I. Cannavaro, D. Roncato, B. Martorana, M. Gosso, *IOP Conference Series: Mater. Sci. Eng.* **2012**, *40*, 012018.
- [101] H. Kim, A. A. Abdala, C. W. Macosko, *Macromolecules* **2010**, *43*, 6515.
- [102] M. Liebscher, M.-O. Blais, P. Pötschke, G. Heinrich, *Polymer* **2013**, *54*, 5875.
- [103] P. K. S. Mural, A. Banerjee, M. S. Rana, A. Shukla, B. Padmanabhan, S. Bhadra, G. Madras, S. Bose, *J. Mater. Chem. A* **2014**, *2*, 17635.
- [104] Y. Cao, J. Zhang, J. Feng, P. Wu, *ACS Nano* **2011**, *5*, 5920.
- [105] C. Mao, Y. Zhu, W. Jiang, *ACS Appl. Mater. Interfaces.* **2012**, *4*, 5281.
- [106] J. Yang, C. Feng, J. Dai, N. Zhang, T. Huang, Y. Wang, *Polym. Int.* **2013**, *62*, 1085.
- [107] A. K. Geim, K. S. Novoselov, *Nat Mater* **2007**, *6*, 183.

- [108] Y. Zhu, S. Murali, W. Cai, X. Li, J. W. Suk, J. R. Potts, R. S. Ruoff, *Adv. Mater.* **2010**, *22*, 3906.
- [109] A. Paydayesh, A. Arefazar, A. Jalaliarani, *J. Appl. Polym. Sci.* **2016**, *133*, 34.
- [110] I. Kelnar, J. Kratochvíl, L. Kaprálková, Z. Špitálský, M. Ujčič, A. Zhigunov, M. Nevoralová, *Polym.-Plast. Technol. Eng.* **2018**, *57*, 827.
- [111] A. Gödel, G. R. Kasaliwal, P. Pötschke, G. Heinrich, *Polymer* **2012**, *53*, 411.
- [112] X. Zhao, J. Zhao, J.-P. Cao, D. Wang, G.-H. Hu, F. Chen, Z.-M. Dang, *Mater. Des. (1980-2015)* **2014**, *56*, 807.
- [113] M. Liebscher, L. Tzounis, P. Pötschke, G. Heinrich, *Polymer* **2013**, *54*, 6801.
- [114] Y. Zhu, H.-y. Ma, L.-f. Tong, Z.-p. Fang, *J. Zhejiang Univ.Sci. A* **2008**, *9*, 1614
- [115] I. Kelnar, J. Kratochvíl, I. Fortelný, L. Kaprálková, A. Zhigunov, M. Nevoralová, *Polym. Compos.* **2017**, *71*, 271.
- [116] M. Yousfi, S. Livi, A. Dumas, J. Crépin-Leblond, M. Greenhill-Hooper, J. Duchet-Rumeau, *J. Appl. Polym. Sci.* **2014**, *131*, 40453.
- [117] R. Salehiyan, T. Malwela, S. S. Ray, *Polym. Degrad. Stabil.* **2017**, *139*, 130.
- [118] G. Filippone, S. Carroccio, G. Curcuruto, E. Passaglia, C. Gambarotti, N. T. Dintcheva, *Polymer* **2015**, *73*, 102.
- [119] G. Filippone, S. Carroccio, R. Mendichi, L. Gioiella, N. T. Dintcheva, C. Gambarotti, *Polymer* **2015**, *72*, 134.
- [120] P. Van Puyvelde, P. Moldenaers, *Rheol. Rev.* **2005**, *2005*, 101.
- [121] P. Van Puyvelde, S. Velankar, P. Moldenaers, *Curr. Opin. Colloid Interface Sci.* **2001**, *6*, 457.
- [122] A. W. Nienow, M. Edwards, N. Harnby, "Mixing in the process industries", Butterworth-Heinemann, 1997.
- [123] F. Fenouillot, P. Cassagnau, J. C. Majesté, *Polymer* **2009**, *50*, 1333.
- [124] D. P. Dharaiya, S. C. Jana, *J. Polym. Sci., Part B: Polym. Phys.* **2005**, *43*, 3638.
- [125] D. P. Dharaiya, S. C. Jana, S. F. Lyuksyutov, *Polym. Eng. Sci.* **2006**, *46*, 19.
- [126] Y. Li, H. Shimizu, *Macromolecules* **2008**, *41*, 5339.
- [127] N. O. Jaensson, C. Mitrias, M. A. Hulsen, P. D. Anderson, *Langmuir* **2018**, *34*, 1795.
- [128] S. Levine, B. D. Bowen, S. J. Partridge, *Colloids Surf.* **1989**, *38*, 325.
- [129] B. P. Binks, *Curr. Opin. Colloid Interface Sci.* **2002**, *7*, 21.
- [130] R. Aveyard, B. P. Binks, J. H. Clint, *Adv. Colloid Interface Sci.* **2003**, *100–102*, 503.
- [131] E. J. Stancik, G. G. Fuller, *Langmuir* **2004**, *20*, 4805.
- [132] C. Sirisinha, N. Prayoonchatphan, *J. Appl. Polym. Sci.* **2001**, *81*, 3198.
- [133] L. Liu, Y. Wang, Y. Li, J. Wu, Z. Zhou, C. Jiang, *Polymer* **2009**, *50*, 3072.
- [134] G. C. Nayak, S. Sahoo, R. Rajasekar, C. K. Das, *Composites, Part A* **2012**, *43*, 1242.
- [135] F. Tao, B. Nysten, A.-C. Baudouin, J.-M. Thomassin, D. Vuluga, C. Detrembleur, C. Bailly, *Polymer* **2011**, *52*, 4798.
- [136] B. Du, U. A. Handge, S. Majeed, V. Abetz, *Polymer* **2012**, *53*, 5491.
- [137] A. Bharati, R. Cardinaels, J. W. Seo, M. Wübberhorst, P. Moldenaers, *Polymer* **2015**, *79*, 271.
- [138] X. Zhao, H. Wang, Z. Fu, Y. Li, *ACS Appl. Mater. Interfaces.* **2018**, *10*, 8411
- [139] W. Xie, Z. Gao, W.-P. Pan, D. Hunter, A. Singh, R. Vaia, *Chem. Mater.* **2001**, *13*, 2979.
- [140] V. Ojijo, H. Cele, S. Sinha Ray, *Macromol. Mater.Eng.* **2011**, *296*, 865.
- [141] E. Moghimi, F. Goharpey, R. Foudazi, *Rheol. Acta* **2014**, *53*, 165.
- [142] B. Krasovitski, A. Marmur, *J. Adhes.* **2005**, *81*, 869.
- [143] D. Wu, L. Wu, W. Zhou, Y. Sun, M. Zhang, *Journal of Polymer Science Part B: Polymer Physics* **2010**, *48*, 479.
- [144] J. Guo, N. Briggs, S. Crossley, B. P. Grady, *Journal of Thermoplastic Composite Materials* **2018**, *31*, 110.

- [145] S. Maiti, S. K. De, A. K. Bhowmick, *Rubber Chem. Technol.* **1992**, *65*, 293.
- [146] A. E. Zaikin, R. R. Karimov, V. P. Arkhireev, *Colloid J.* **2001**, *63*, 53.
- [147] J. Plattier, L. Benyahia, M. Dorget, F. Niepceon, J.-F. Tassin, *Polymer* **2015**, *59*, 260.
- [148] A. L. Persson, H. Bertilsson, *Polymer* **1998**, *39*, 5633.
- [149] Z.-Y. Xiong, L. Wang, Y. Sun, Z.-X. Guo, J. Yu, *Polymer* **2013**, *54*, 447.
- [150] J. Feng, C.-m. Chan, J.-x. Li, *Polym. Eng. Sci.* **2003**, *43*, 1058.
- [151] H. H. Le, I. Prodanova, S. Ilisch, H.-J. Radusch, *Rubber Chem. Technol.* **2004**, *77*, 815.
- [152] N. Najafi, M. C. Heuzey, P. J. Carreau, P. M. Wood-Adams, *Polym. Degrad. Stabil.* **2012**, *97*, 554.
- [153] M. Kruse, M. H. Wagner, *Rheol. Acta* **2016**, *55*, 789.
- [154] E. Chiellini, A. Corti, S. D'antone, R. Baciú, *Polym. Degrad. Stabil.* **2006**, *91*, 2739.
- [155] S. Kirkpatrick, *Rev. Mod. Phys.* **1973**, *45*, 574.
- [156] J. R. Miller, *J. Chem. Phys.* **1972**, *56*, 5173.
- [157] P. Sheng, E. K. Sichel, J. I. Gittleman, *Phys. Rev. Lett.* **1978**, *40*, 1197.
- [158] C. Tang, N. Chen, X. Hu, "Conducting Polymer Nanocomposites: Recent Developments and Future Prospects", in *Conducting Polymer Hybrids*, V. Kumar, S. Kalia, and H.C. Swart, Eds., Springer International Publishing, Cham, **2017**, p. 1.
- [159] I. Balberg, S. Bozowski, *Solid State Commun.* **1982**, *44*, 551.
- [160] S. J. Babinec, R. D. Mussell, R. L. Lundgard, R. Cieslinski, *Adv. Mater.* **2000**, *12*, 1823.
- [161] S. H. Munson-McGee, *Phys. Rev. B* **1991**, *43*, 3331.
- [162] J. Fournier, G. Boiteux, G. Seytre, G. Marichy, *Synth. Met.* **1997**, *84*, 839.
- [163] J. N. Coleman, S. Curran, A. Dalton, A. Davey, B. McCarthy, W. Blau, R. Barklie, *Phys. Rev. B* **1998**, *58*, R7492.
- [164] S. D. McCullen, D. R. Stevens, W. A. Roberts, S. S. Ojha, L. I. Clarke, R. E. Gorga, *Macromolecules* **2007**, *40*, 997.
- [165] H. Deng, T. Skipa, E. Bilotti, R. Zhang, D. Lellinger, L. Mezzo, Q. Fu, I. Alig, T. Peijs, *Adv. Funct. Mater.* **2010**, *20*, 1424.
- [166] G. Pike, C. Seager, *Phys. Rev. B* **1974**, *10*, 1421.
- [167] C. Seager, G. Pike, *Phys. Rev. B* **1974**, *10*, 1435.
- [168] A. Dani, A. A. Ogale, *Compos. Sci. Technol.* **1996**, *56*, 911.
- [169] I. Balberg, N. Binenbaum, *Phys. Rev. B* **1983**, *28*, 3799.
- [170] M. Grujicic, G. Cao, W. Roy, *J. Mater. Sci.* **2004**, *39*, 4441.
- [171] M. Foygel, R. Morris, D. Anez, S. French, V. Sobolev, *Phys. Rev. B* **2005**, *71*, 104201.
- [172] J. Li, J.-K. Kim, *Compos. Sci. Technol.* **2007**, *67*, 2114.
- [173] E. M. Sevick, P. A. Monson, J. M. Ottino, *J. Chem. Phys.* **1988**, *88*, 1198.
- [174] R. Taipalus, T. Harmia, M. Q. Zhang, K. Friedrich, *Compos. Sci. Technol.* **2001**, *61*, 801.
- [175] H. Pang, L. Xu, D.-X. Yan, Z.-M. Li, *Prog. Polym. Sci.* **2014**, *39*, 1908.
- [176] M. Sumita, K. Sakata, Y. Hayakawa, S. Asai, K. Miyasaka, M. Tanemura, *Colloid Polym. Sci.* **1992**, *270*, 134.
- [177] S. Srivastava, R. Tchoudakov, M. Narkis, *Polym. Eng. Sci.* **2000**, *40*, 1522.
- [178] B. G. Soares, F. Gubbels, R. Jérôme, P. Teyssié, E. Vanlathem, R. Deltour, *Polym. Bull.* **1995**, *35*, 223.
- [179] M. Gültner, A. Gödel, P. Pötschke, *Compos. Sci. Technol.* **2011**, *72*, 41.
- [180] J. Huang, C. Mao, Y. Zhu, W. Jiang, X. Yang, *Carbon* **2014**, *73*, 267.
- [181] J. Chen, X. Cui, Y. Zhu, W. Jiang, K. Sui, *Carbon* **2017**, *114*, 441.
- [182] J.-F. Gao, D.-X. Yan, B. Yuan, H.-D. Huang, Z.-M. Li, *Compos. Sci. Technol.* **2010**, *70*, 1973.

- [183] I. Sagalianov, L. Vovchenko, L. Matzui, O. Lazarenko, *Nanoscale Res. Lett.* **2017**, *12*, 140.
- [184] P. Pötschke, B. Kretzschmar, A. Janke, *Compos. Sci. Technol.* **2007**, *67*, 855.
- [185] P. Pötschke, A. R. Bhattacharyya, A. Janke, *Polymer* **2003**, *44*, 8061.
- [186] J. Chen, Y. Shen, J.-h. Yang, N. Zhang, T. Huang, Y. Wang, Z.-w. Zhou, *J. Mater. Chem C* **2013**, *1*, 7808.
- [187] J. Chen, H.-y. Lu, J.-h. Yang, Y. Wang, X.-t. Zheng, C.-l. Zhang, G.-p. Yuan, *Compos. Sci. Technol.* **2014**, *94*, 30.
- [188] J. Chen, Y.-y. Shi, J.-h. Yang, N. Zhang, T. Huang, C. Chen, Y. Wang, Z.-w. Zhou, *J. Mater. Chem.* **2012**, *22*, 22398.
- [189] A. V. Poyekar, A. R. Bhattacharyya, R. A. Khare, A. S. Panwar, G. P. Simon, S. Dhar, J. K. Mishra, *Polym. Eng. Sci.* **2015**, *55*, 443.
- [190] N. Antonio Castro, G. Francisco, P. Nuno Miguel, *Phys. World* **2006**, *19*, 33.
- [191] V. Singh, D. Joung, L. Zhai, S. Das, S. I. Khondaker, S. Seal, *Prog. Mater. Sci.* **2011**, *56*, 1178.
- [192] V. D. Punetha, S. Rana, H. J. Yoo, A. Chaurasia, J. T. McLeskey Jr, M. S. Ramasamy, N. G. Sahoo, J. W. Cho, *Prog. Polym. Sci.* **2017**, *67*, 1.



Dr. Reza Salehiyan received his PhD in chemical engineering from Pusan National University, Pusan, South Korea, in 2016. Currently, he is working with Prof. Suprakas Sinha Ray's research group as a postdoctoral fellow. His research work focuses on the effects of nanoparticle localization and geometry on the thermal degradation kinetics and electrical and dielectric properties of immiscible blends, in association with their rheological properties.



Prof. Suprakas Sinha Ray is Chief Researcher in Polymer Nanocomposites at the Council for Scientific and Industrial Research (CSIR), Pretoria, South Africa. He was awarded a PhD in physical chemistry by the University of Calcutta in 2001 and is Director of the Department of Science and Technology (DST)-CSIR National Center for Nanostructured Materials. He is also affiliated with the University of Johannesburg as a Distinguished Visiting Professor of Applied Chemistry. Prof. Ray's current research focus is on polymer-based advanced nanostructured materials and their applications.